Quantification of ice production in Laptev Sea polynyas and its sensitivity to thin-ice parameterizations in a regional climate model

Oliver Gutjahr[1], Günther Heinemann[1], Andreas Preußer[1], Sascha Willmes[1], and Clemens Drüe[1]

[1]Department of Environmental Meteorology, University of Trier, Behringstraße 21, 54296 Trier, Germany

Correspondence to: Oliver Gutjahr (gutjahr@uni-trier.de)

Abstract. The quantification of sea-ice production in the Laptev Sea polynyas is important for the Arctic sea-ice budget and the heat loss to the atmosphere. We estimated the ice production for the winter season 2007/08 (Nov.-Apr.) based on simulations with the regional climate model COSMO-CLM at a horizontal resolution of 5 km and compared it to remote sensing estimates. A reference and five sensitivity simulations were performed with different assumptions on grid-scale and subgrid-scale ice thickness considered within polynyas, using a tile approach for fractional sea ice. In addition, the impact of heat loss on the atmospheric boundary layer was investigated.

About $29.1 \, \mathrm{km}^3$ of total winter ice production was estimated for the reference simulation which varies by up to $+124\%$ in dependence on the thin-ice assumptions. For the most realistic assumptions based on remote sensing of ice thickness the ice production increases by $+39\%$. The use of the tile-approach enlarges the area and enhances the magnitude of the heat loss from polynyas up to $+110\%$ if subgrid-scale open-water is assumed, and by $+20\%$ for realistic assumptions. This enhanced heat loss causes in turn higher ice production rates and stronger impact on the atmospheric boundary layer structure over the polynyas. The study shows that ice production is highly sensitive to the thin-ice parameterizations for fractional sea ice cover. In summary, realistic ice production estimates could be retrieved from our simulations. Neglecting subgrid-scale energy fluxes might considerably underestimate the ice production in coastal polynyas, such as in the Laptev Sea, with possible consequences on the Arctic sea-ice budget.

1 Introduction

The rate of sea-ice growth strongly depends on the energy fluxes at the ice or ocean surface. If the total atmospheric heat flux is negative, the ocean loses heat either directly to the atmosphere or via conduction through an existing sea-ice cover. In the former case frazil ice forms, which aggregates subsequently to a new thin-ice layer under calm conditions. In the latter case basal freezing occurs to balance this heat loss. Most of the heat loss from the ocean occurs over open-water or thin-ice areas, such as leads and polynyas, within an otherwise compact sea-ice cover (Smith et al., 1990; Morales Maqueda et al., 2004). Although the fraction of such areas in polar oceans is relatively small during winter, they are of major importance for the heat budget of the atmospheric boundary layer (ABL) (Heinemann and Rose, 1990; Haid et al., 2015) and the ocean circulation, such as the Arctic circumpolar boundary current (e.g. Aksenov et al., 2011; Rudels et al., 1999).
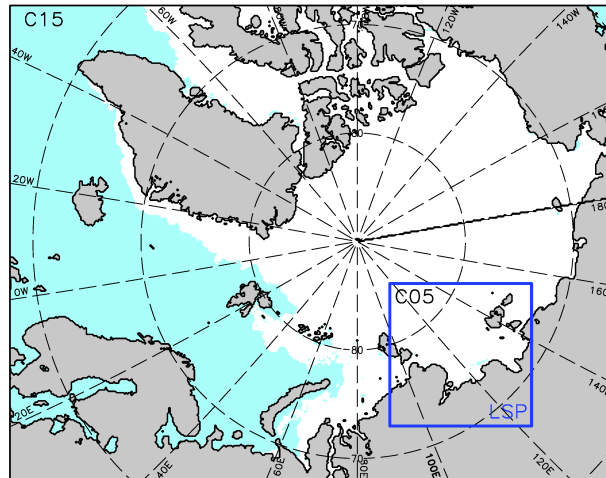
Figure 1. Model domains of COSMO-CLM at a horizontal resolution of $15\,\text{km}$ (C015, whole Arctic). The study domain of the Laptev Sea polynyas (LSP) with a resolution of $5\,\text{km}$ (C05, blue box) is shown in detail in Fig. 2. The sea-ice extent (white shaded) is from 4 January 2008.

The Laptev Sea (Siberia) is a very shallow shelf sea with water depths between 15 and 200 m and comprises an area of about $500 \times 10^3\,\text{km}^2$ (Timokhov, 1994; Krumpen et al., 2013). It is one of the most significant regions where a considerable amount of the total Arctic sea ice is produced (Aagard et al., 1981; Dmitrenko et al., 2009; Dethleff et al., 1998; Willmes et al., 2011; Tamura and Ohshima, 2011; Iwamoto et al., 2014). The newly formed sea ice is subsequently transported by the Transpolar
5 Drift System and accounts for about 20 % of the total ice export through Fram Strait (Rigor and Colony, 1997). The Laptev Sea thus plays a key role for future Arctic sea-ice development (Krumpen et al., 2013).

Quasi-stationary latent-heat or flaw polynyas reoccur frequently along the Sibirian coast and along the fast ice edge (Dmitrenko et al., 2001; Krumpen et al., 2011; Bareiss and Görgen, 2005) due to offshore wind stress (Smith et al., 1990; Dmitrenko et al., 2001; Morales Maqueda et al., 2004; Krumpen et al., 2011; Willmes et al., 2011; Dmitrenko et al., 2012). These polynyas
10 are narrow, long bands of open water and/or thin-ice, which separate landfast ice from seaward drifting ice on the Siberian continental shelves during winter (Dethleff et al., 1998), predominantly from October until June (Bareiss and Görgen, 2005). In general, the ice cover in the Laptev Sea can be divided into three regimes: fast ice, pack ice, and flaw polynyas in between (Eicken et al., 2005).

Particularly in winter, sea water at the freezing point is directly exposed to a cold atmosphere, resulting in intense ice
15 formation (Dethleff et al., 1998). Owing to this strong surface heat loss within coastal polynyas frazil ice forms, which is subsequently transported toward the downwind edge of the polynyas (Smith et al., 1990; Morales Maqueda et al., 2004; Krumpen et al., 2011; Willmes et al., 2010). This process creates a spatial gradient of thin-ice thickness (TIT) increasing from open-water conditions at the windward polyna edge to thicker ice at the downwind side. Here, at the polynya edge, the advected
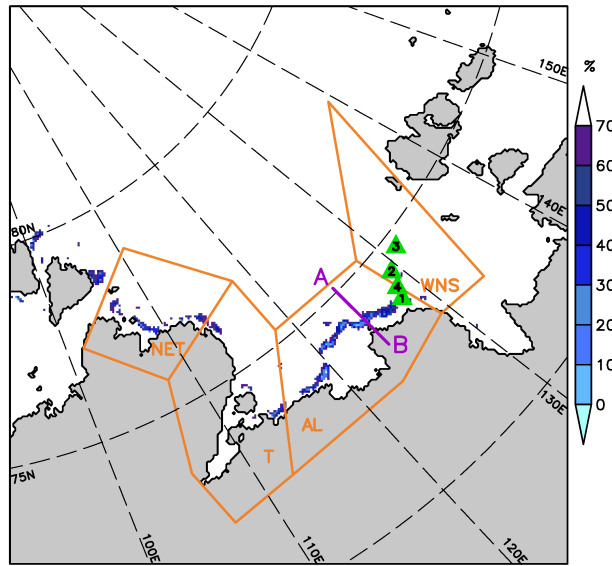
Figure 2. Model domain at $5\,\mathrm{km}$ resolution (C05) over the Laptev Sea (approximately $1500\,\mathrm{km} \times 1500\,\mathrm{km}$) with the sea-ice concentration from AMSR-E showing open polynyas ($\leq 70\,\%$) on 4 January 2008. Four polynya regions are superimposed as orange polygons: northeastern Taimyr polynya (NET), the Taimyr polynya (T), the Anabar-Lena polynya (AL) and the western New Siberian polynya (WNS). A→B denotes the $214\,\mathrm{km}$ long cross-section (magenta) used in section 5. The locations of the four AWS stations are marked with green triangles.

frazil ice accumulates to a thin layer (Martin and Kauffmann, 1981; Krumpen et al., 2011), which thickens and consolidates before it drifts further offshore. During the ice formation, salt is excluded from the ice matrix and is drained as brine from the sea ice (Krumpen et al., 2011). This salt input induces haline convection and erodes the density stratification of the underlying water column (Ivanov and Golovin, 2007; Bauch et al., 2009) and if penetrative, dense bottom water forms (Backhaus et al.,

5 1997; Bauch et al., 1995). The long-term mean probability for convective mixing down to the seafloor is only about $20\,\%$ in the western and about $70\,\%$ in the eastern Laptev Sea (Dmitrenko et al., 2005; Krumpen et al., 2011), which is owed to the general preservation of the stratification throughout the winter caused by freshwater input from the Lena River during summer (Bauch et al., 2009; Dmitrenko et al., 2005). The cold, dense bottom water contributes to the Arctic halocline (Bauch et al., 2009) and thermohaline structure in the Eurasian Basin (Johnson and Polyakov, 2001).

10 The horizontal resolution of regional climate models is generally too coarse to represent leads and small polynyas explicitly. Therefore, they have to be treated as inhomogeneities of momentum and energy fluxes on a subgrid scale. Heinemann and Kerschgens (2005) investigated three approaches to account for such subgrid-scale inhomogeneities within a model grid box: the (i) aggregation, (ii) mosaic and (iii) tile-approach (TA). In the aggregation approach the parameters for the fluxes (such as roughness length or albedo) are weight-averaged over different surface types within a grid box and then the fluxes are
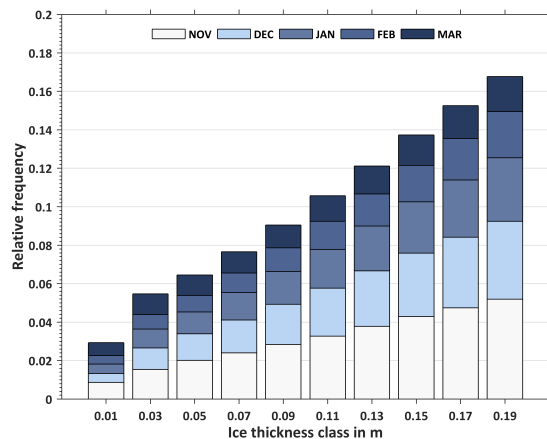
Figure 3. Thin-ice thickness distribution ($\leq 20\,\text{cm}$) in the Laptev Sea derived from MODIS data for the winter periods (Nov.-Mar.) 2002/03–2014/15. The bars indicate the relative distribution of each thickness class from the total number of TIT $\leq 0.2\,\text{m}$ appearances between the winter seasons 2002/03 and 2014/15. Contributions of each month with respect to the whole winter season for each thickness class are indicated by the blueish colors (see the legend). The mean thickness ($\pm$ one standard deviation) in this period is $13.5 \pm 0.5\,\text{cm}$ ($8.7\,\text{cm}$ for $\leq 10\,\text{cm}$). In the winter period 2007/08, the mean is $14.0 \pm 2\,\text{cm}$ ($7.7\,\text{cm}$ for $\leq 10\,\text{cm}$).

calculated from these grid-scale means. In contrary, in the mosaic approach the fluxes are explicitly calculated on a sub-scale grid and averaged afterwards. In the standard version (v5.0_clm1) of the regional climate model 'COnsortium for Small-scale MOdel - Climate Limited area Mode' (COSMO-CLM or CCLM; Rockel et al. (2008)), which is the climate version of the numerical weather prediction model COSMO of the German Meteorological Service (Steppeler et al., 2003), a model grid

5 box is either assumed to be completely covered with sea ice or to be completely ice-free. However, if neglecting subgrid-scale energy fluxes or heat loss from open-water or thin-ice areas, the energy transfer is underestimated and subsequently also the sea-ice production. This underestimation affects the sea-ice budget and associated processes connected to the ocean, such as salt release and deep water formation (Martin and Cavalieri, 1989; Bauch et al., 1995; Ivanov and Golovin, 2007). Although the ocean processes are not represented in CCLM, the quantification of sea-ice production can be seen as a proxy for dense

10 water formation.

In other regional climate models, such as the Polar Weather Research & Forecasting (Polar-WRF) Model, fractional sea ice is already a default option with the assumption of subgrid-scale open water and with fixed sea-ice concentrations (SIC) and ocean temperatures during a 48 h simulation (Bromwich et al., 2009). However, assumptions have to be made for the subgrid-scale thin-ice thickness, since particularly in winter leads and polynyas are rarely ice-free (Willmes et al., 2011, 2010; Adams

15 et al., 2013).

In the following we quantify the sea-ice production in the Laptev Sea polynyas (Siberia) and investigate its sensitivity on the assumptions of thin-ice thickness associated with the tile-approach. The sea-ice module of Schröder et al. (2011) was

Table 1. Overview of the performed simulations with COSMO-CLM for the winter period 2007/11–2008/04. The grid-scale thin-ice thickness (TIT) within polynyas (ice concentration: $0 < SIC \leq 70\%$) is shown in cm and the assumed subgrid-scale TIT is shown in parenthesis. The latter is only required if the tile-approach (TA) is used.

Model run	Δx	Region	TIT [cm]	TA	Information
C15	15 km	Arctic	10 (-)	no	forced by ERA-Interim
C05-ref	5 km	Laptev Sea	10 (-)	no	reference run
C05-10/0	5 km	Laptev Sea	10 (0)	yes	subgrid-scale open-water
C05-10/1	5 km	Laptev Sea	10 (1)	yes	
C05-10/10	5 km	Laptev Sea	10 (10)	yes	
C05-50/5	5 km	Laptev Sea	50 (5)	yes	
C05-50/1	5 km	Laptev Sea	50 (1)	yes	realistic assumptions

already successfully applied in the Laptev Sea by Ebner et al. (2011), who could show that polynyas significantly affect the atmospheric boundary layer. More recently, Bauer et al. (2013) calculated sea-ice production rates for this region based on COSMO simulations with an assumed thin-ice thickness of 10 cm (B10) or open water (B00) within polynyas. Their model results showed that the presence of grid-scale thin-ice affects the IP considerably.

5 The implementation of a TA for subgrid-scale energy fluxes constitutes, from a physical point of view, an improvement of representing polynyas in regional climate models. However, it is unclear how sensitive the energy fluxes, the resulting IP, and the ABL are to the choice of grid-scale and subgrid-scale ice thickness. By varying the thin-ice thickness in a sensitivity experiment, we aim to quantify these uncertainties. As a benchmark for our study we use the IP estimations of Willmes et al. (2011). We further comprise model results of Bauer et al. (2013) and derived IP from Moderate Resolution Imaging
10 Spectroradiometer (MODIS) data.

  This paper is structured as follows: in section 2, a short overview of the model configuration and the study region is given; in section 3 the basics of the sea-ice module are described (see details in appendix A and appendix B). The model is validated with in situ data in section 4 and the effects on the atmospheric boundary layer and on ice production rates are presented in section 5 and 6 and discussed with respect to remote sensing estimates in section 7. Finally, we conclude in section 8.

15 ## 2 CCLM configuration and model domains

The domain of CCLM (Fig. 1) covers the whole Arctic at a horizontal resolution of 15 km (C15). CCLM was run on 450×350 grid boxes and with 42 vertical layers, whereof 16 are below 2 km height. Nested within, we performed simulations for the Laptev Sea (Fig. 2 and Tab.1) at 5 km resolution (C05) with 260×260 grid boxes and 60 vertical levels, whereof 24 levels are below 2 km height. We subdivided this domain into four polynya regions, which have been already used in previous studies,
20 e.g. by Willmes et al. (2011): the north-eastern Taimyr polynya (NET), the Taimyr polynya (T), the Anabar-Lena polynya (AL) and the western New Siberian polynya (WNS). The total area of the masks is $26.19 \times 10^4 \, km^2$.

The C15 model is forced by ERA-Interim data (Dee et al., 2011) with updates to the lateral boundaries every 6 h. The C05 models are then forced by the output of C15 with an update frequency of 1 h. The models were run in a forecasting procedure for the winter period November 2007 to April 2008 (182 days in total). They were restarted every simulation day at 18 UTC and simulated the following 30 hours. Thereby the initial sea-ice conditions (see section 3.2) were prescribed to the sea-ice
5   concentration and thickness of the following day. The first 6 hours were cut off as spin-up. The simulation output (00-23 UTC) was stored at a temporal resolution of 1 hour.

Surface fluxes were calculated by a bulk transfer scheme with a stability dependence (Louis, 1979) (see appendix B3). The vertical diffusion was parameterized by a level-2.5 closure scheme (Mellor and Yamada, 1974) based on a prognostic equation for turbulent kinetic energy (TKE). Radiation processes were calculated hourly uing the Ritter and Geleyn (1992)
10   scheme extended for ice-clouds. We applied a Runge-Kutta scheme of 3rd order (Wicker and Skamarock, 2002). Additionally, a fast-wave solver for sound and gravity waves was used (Baldauf, 2013). All simulations were run without spectral nudging.

To improve the simulation of heat loss over fractional sea ice in CCLM, we modified the standard version with regard to the following points: (i) we implemented the thermodynamic 2-layer sea-ice module of Schröder et al. (2011), (ii) we used daily sea-ice thickness (SIT) fields from the Pan-Arctic Ice-Ocean Modeling and Assimilation System (PIOMAS) data set
15   (Zhang and Rothrock, 2003) as initial data, (iii) we implemented a new albedo-scheme for sea ice based on Køltzow (2007), and (iv) we implemented a tile-approach for the energy balance over fractional sea ice. The TA is a simplification of the mosaic approach, considering only the percentage of different surface types but not their exact location. According to Heinemann and Kerschgens (2005) the TA provides similarly good results as the mosaic approach, but with distinctly less computation time. Thus, we decided to implement this variant. First steps in the direction of a tile-approach in CCLM were made by Van Pham
20   et al. (2014). However, their adjustments were limited to area-weighted albedo values and to surface roughness values within a grid box that is covered with fractional sea ice. Although points (ii)-(iii) represent new modifications to CCLM as well, we accept them as the default option for our simulations.

The C15 simulation was performed without a TA in order to introduce effects from the TA only through the 5 km simulations. In case of C05, we performed a reference simulation in the Laptev Sea area without a TA (C05-ref) and five sensitivity
25   simulations with the TA. The configuration of the reference simulation is similar (as far as possible) to the configuration of the previous studies of Bauer et al. (2013), where no TA was available. However, they used an older model version which causes differences. C05-ref is thus comparable to the simulations of Bauer et al. (2013) and further the reference without TA for our sensitivity simulations.

While the sea-ice thickness outside the polynyas was specified as explained in section 3.2, the ice thickness within the
30   polynya areas has to be prescribed. For C15 and C05-ref the ice thickness in polynyas areas is generally 10 cm, but we assume 1 cm thin ice at polynya grid boxes in C05-ref, where the sea-ice concentration is 0 %. Such areas particularly produce new ice and consist of a mixture of open water, grease and frazil ice, and thin solid ice. However, in winter open-water areas occur mostly at the windward side of polynyas, which is only a small fraction of the entire polynya area.

For three of the five sensitivity simulations we assumed also a grid-scale ice thickness of 10 cm for polynyas and either
35   assumed subgrid-scale open water (C05-10/0) or a subgrid-scale TIT of 1 cm (C05-10/1) and 10 cm (C05-10/10), respectively.
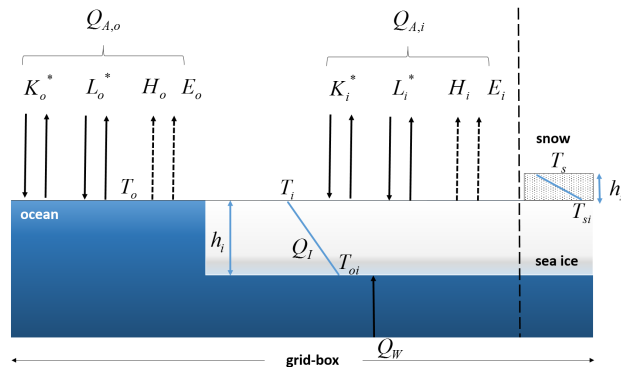
Figure 4. Scheme of the modified two-layer thermodynamic sea-ice module of Schröder et al. (2011), extended with a tile-approach for fractional sea ice. Sea ice is distinguished as bare ice or as snow covered ice (with $h_s = 0.1\,\mathrm{m}$ snow depth if sea-ice thickness $h_i > 0.2\,\mathrm{m}$). The subgrid-scale open ocean fraction is either ice-free (C05-10/0) or assumed to be covered with $1\,\mathrm{cm}$ (C05-10/1, C05-50/1), $5\,\mathrm{cm}$ (C05-50/5) or $10\,\mathrm{cm}$ thin-ice (C05-10/10). In the reference simulation (C05-ref), grid boxes with $0\,\%$ sea-ice concentration are covered with 1 cm grid-scale thin-ice. If the index k denotes either sea-ice (i) or ocean (o), then $Q_{A,k}$ is the total atmospheric heat flux, K_k^* is the net shortwave and L_k^* the net longwave radiation. H_k and E_k are the sensible and latent heat fluxes. T_k is the surface temperature, h_i the ice thickness, T_{oi} the ice-ocean interface temperature and T_{si} the snow-ice interface temperature. Q_I denotes the conductive heat flux through the ice and Q_W the turbulent heat flux from the oceanic mixed layer into the ice.

The fourth and fifth sensitivity simulations were configured with a grid-scale ice thickness of $50\,\mathrm{cm}$ and a subgrid-scale TIT of $5\,\mathrm{cm}$ (C05-50/5) or $1\,\mathrm{cm}$ (C05-50/1). See Tab. 1 for an overview of the simulations. The assumption of 10 cm TIT originates from the fact that the mean TIT below $20\,\mathrm{cm}$, derived from MODIS data, is of the order of $\approx 10\,\mathrm{cm}$. Willmes et al. (2011) derived a mean thin-ice thickness of 11.6 cm for November to April (1979-2008), while from the MODIS TIT histogram in Fig.3, a mean thin-ice thickness of 13.5 cm for November to March in the period 2002/03–2014/15 and of 14 cm for the winter 2007/08 results, respectively. In a previous study by Bauer et al. (2013) 10 cm was thus assumed to be a realistic value for the thin-ice thickness within Laptev Sea polynyas. For better comparisons we assumed 10 cm as well in our reference simulation (and in two sensitivity runs).

The first three sensitivity simulations investigate the effect of the TA, if even thinner sub-grid scale ice is assumed. The C05-50/5 and C05-50/1 runs are motivated by the fact that the sea-ice cover in the marginal ice zone consists of thicker ice floes ($> 20\,\mathrm{cm}$) (detected by microwave satellite sensors), and thin-ice (here the assumed 5 cm or 1 cm), which is not detected by microwave sensors. Thus we denote C05-50/1 as the simulation with 'realistic' assumptions based on MODIS TIT.

Although this is a crude simplification to the real sea-ice thickness, it is suited for our purpose to investigate the impact on the magnitude of ice production and on the modification of the ABL. We intended to consider sea ice in a computational cheap approach that still incorporates realistic thermo-dynamical processes. For a more sophisticated approach, a full dynamic-thermodynamic sea-ice model needs to be coupled to CCLM.

3 The two-layer thermodynamic sea-ice module

3.1 Basic module

In this section the sea-ice module (Fig. 4) is briefly described. The module considers a snow and sea ice layer and was described and originally implemented in the COSMO model by Schröder et al. (2011). It is based on the module of Mironov et al. (2012).

5 For this study it is reimplemented within the version 5.0_clm1 of CCLM extended with the Køltzow sea-ice albedo scheme (see appendix A). More important for this study is the implementation of a tile-approach for the surface energy balance over fractional sea ice (see appendix B). The module and hence sea-ice growth calculation is only applied to grid boxes with an initial sea-ice cover. Formation of grease ice in open water is not parameterized in CCLM, which is even a difficult task for stand-alone sea-ice ocean models. Nevertheless, a more sophisticated parameterization has been recently developed by

10 Smedsrud and Martin (2015). For this reason we calculated sea-ice production in a post-processing step (see section 3.4).

The module assumes a constant ocean/ice interface temperature of $T_{oi} = -1.7\,^{\circ}$C, i.e. T_{oi} is not dependent on salinity. A temperature of $-1.7\,^{\circ}$C assumes approximately a salinity of $31.1\,$psu. The module ignores turbulent heat fluxes from the ocean at the lower boundary. Heat conductivity parameters are $2.3\,\mathrm{W\,m^{-1}K^{-1}}$ for sea ice and $0.76\,\mathrm{W\,m^{-1}K^{-1}}$ for snow. The module assumes a snow cover of $h_s = 0.1\,$m if the ice thickness exceeds a threshold $h_i > h_c$ with $h_c = 0.2\,$m.

15 ### 3.2 Sea-ice concentration and thickness for initial conditions

The sea-ice concentration (SIC) is prescribed from Advanced Microwave Scanning Radiometer-Earth Observing System (AMSR-E) data (Spreen et al., 2008), provided by the University of Bremen. The original data sets are available on a daily basis at a horizontal resolution of 6.25 km. In order to use them for CCLM, we interpolated the SIC fields onto the C15 and C05 grid, respectively, by a bilinear approach for every simulation day. All grid boxes with SIC $\leq 70\,\%$ are treated as polynyas

20 (Massom et al., 1998; Adams et al., 2011; Preußer et al., 2015a). Realistic polynya areas are retrieved by using this threshold, as shown by Adams et al. (2011) in comparison to a polynya signature simulation method (Markus and Burns, 1995).

Sea-ice thickness (SIT) is taken from the Pan-Arctic Ice-Ocean Modeling and Assimilation System (PIOMAS) data set (Zhang and Rothrock, 2003). The PIOMAS data are available at a daily basis with a mean grid spacing of about 25 km (Hines et al., 2015). These daily fields were masked with the daily SIC fields to obtain consistent sea-ice extents. Thereby sea ice

25 outside the AMSR-E mask was removed and grid boxes which were ice-free in the daily PIOMAS fields but covered with ice in the mask were assigned with an interpolated SIT from a nearest neighbour method.

Schweiger et al. (2011) state that PIOMAS seems to overestimate thin-ice thickness and underestimates thicker ice. Nevertheless, the overestimation should not be problematic in our application, since we have to set TIT for daily fields according to AMSR-E data. Underestimations of thicker ice is of a minor concern to our study due to the focus on areas with thin ice. Using

30 this setup, the sea-ice thickness fields are much more realistic than in previous studies, where a constant thickness of $1\,$m was assumed outside polynyas (Ebner et al., 2011; Schröder et al., 2011; Bauer et al., 2013).

Table 2. Overview of the four automatic weather stations (AWS) with hourly measurements which were deployed during the Transdrift XIII-2 expedition from 11–29 April 2008 (Heinemann et al., 2009). See the location of the AWS stations in Fig. 2.

Station	Location	Measured period (UTC)
AWS1	128.16 °E	11 Apr. 2008 07:00 – 26 Apr. 2008 12:00
	73.80 °N	
AWS2	129.32 °E	12 Apr. 2008 04:00 – 29 Apr. 2008 03:00
	74.39 °N	
AWS3	131.25 °E	14 Apr. 2008 06:00 – 29 Apr. 2008 01:00
	74.67 °N	
AWS4	128.61 °E	24 Apr. 2008 06:00 – 28 Apr. 2008 02:00
	74.05 °N	

3.3 Polynya area

In Fig. 5 daily polynya areas for the winter period 2007/08 are shown. According to the AMSR-E data set, which has been used to prescribe the SIC in CCLM and in the COSMO simulations of Bauer et al. (2013), large polynya events ($> 10^4 \, \mathrm{km}^2$) occurred at the end of November, in January and in March/April. The polynya areas of Willmes et al. (2011) are approximately
5 of the same order as those used for CCLM, whereas the retrieved polynya areas from MODIS2km are considerably larger. This discrepancy is caused by different threshold definitions for polynyas and by different horizontal resolutions. For the MODIS2km data, polynyas were defined as areas with thin-ice $\leq 20\,\mathrm{cm}$, as in Preußer et al. (2015b). Given that and the higher horizontal resolution it is likely that also leads within the polynya masks, not resolved by the microwave satellite data, are contributing to the total thin-ice area and hence larger areas result. If areas of open-water outside polynyas are considered as
10 well, then the potential area for ice production increases in CCLM up to the area derived from MODIS2km data, except in the period of late November to the mid of January, which remains lower. Another difference between the polynya area derived from CCLM and in particular the area from Willmes et al. (2011) is that the latter nearly never drops to zero during this winter.

3.4 Estimation of sea-ice production

In accordance to previous model or satellite-based studies, the sea-ice production (IP) was calculated in a post-processing
15 step using the energy balance (Bauer et al., 2013; Ebner et al., 2011; Willmes et al., 2011). This approach assumes that if the water within a polynya is at the freezing point, all energy loss to the atmosphere through the ocean surface is compensated by freezing. Hence sea-ice growth only occurs if the total atmospheric energy flux over ice (index $k = i$) or ocean (index $k = o$) $Q_{A,k} = K_k^* + L_k^* + H_k + E_k$ is negative, i.e. the ocean looses heat:

$$\frac{\partial h_i}{\partial t} = -\frac{Q_{A,k}}{\rho_i \cdot L_f}, \tag{1}$$
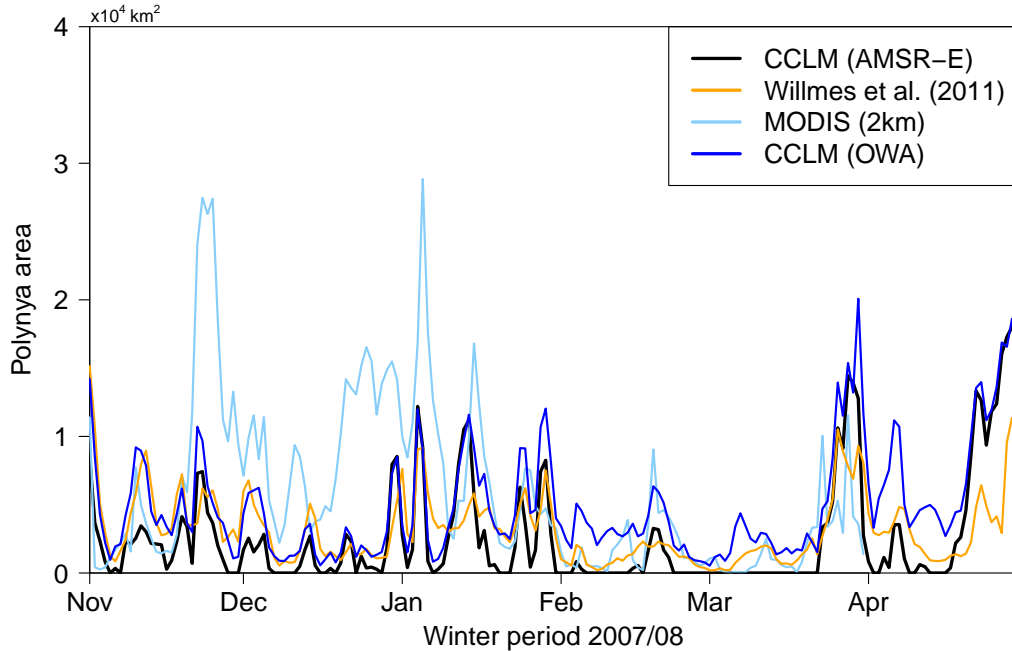
Figure 5. Total daily polynya area interpolated from AMSR-E (using a 70 % threshold) onto the CCLM 5 km grid in the Laptev Sea for the winter period 2007/08 aggregated for the four polynya masks. In addition, the polynya area plus open-water area (OWA $= 1 - $ SIC) for the polynya masks is shown. Based on remote sensing the polynya areas estimated from Willmes et al. (2011) and MODIS2km data are shown. The total area of the polynya masks is $26.19 \times 10^4 \, \mathrm{km}^2$.

with h_i the sea-ice thickness, $\rho_i = 910 \, \mathrm{kg \, m}^{-3}$ the density of sea ice and $L_f = 0.334 \times 10^6 \, \mathrm{J \, kg}^{-1}$ the latent heat of fusion. We restricted this estimation to the four polynya areas in the Laptev Sea (see Fig. 2), which are identical to those of Willmes et al. (2011). Hence, direct comparisons of our results with estimations from remote sensing were possible.

We further calculated the IP using the MOD/MYD29 sea-ice surface temperature product (Hall et al., 2004; Riggs et al.,
5 2006) derived from MODIS Terra and Aqua data. In combination with ERA-Interim data (2 m temperature, 2 m dew point temperature, 10 m horizontal wind components and pressure at mean sea level), an energy balance model (e.g. Yu and Lindsay, 2003; Adams et al., 2013; Preußer et al., 2015b, a) was applied to derive thin-ice thicknesses up to 0.2 m at a horizontal resolution of about 2 km. We refer to this estimation as MODIS2km. The turbulent fluxes of sensible and latent heat were calculated by an iterative bulk approach (Launiainen and Vihma, 1990) based on the Monin-Obukhov similarity theory. Thereby, the tur-
10 bulent exchange coefficient C_H is a function of stability, and of the roughness length for momentum and for heat, respectively (Doms et al., 2011). Shortwave radiation is not considered as the method is restricted to nighttime conditions during winter. This method is only applicable to clear sky conditions, as clouds and fog impede an estimation of sea-ice surface temperature

Table 3. Statistical comparison of $2\,\mathrm{m}$ temperature, $10\,\mathrm{m}$ wind speed ($3\,\mathrm{m}$ in case of the AWS) and net radiation ($K^* + L^*$) of the four AWS and the C05 simulations: C05-ref (reference), C05-10/0 (open-water), and C05-50/1 (realistic). Hourly means are denoted by $\bar{x}$ and standard deviations are denoted by σ. The Pearson correlation coefficient (r) was calculated with the AWS and C05 time series. The critical correlation coefficient ($\alpha = 5\,\%$), which is depending on the sample size of the AWS time series, is between 0.1 and 0.2. In addition, the resulting p-values (p) of two-sided t-tests ($\alpha = 5\,\%$) are shown. Significant differences are marked with *. Data pairs with missing values in the AWS data or where the sea-ice concentration is $< 95\,\%$ were removed prior to the analyses.

Data	2 m temperature (°C)				10 m wind speed (m s^{-1})				net radiation (W m^{-2})			
	$\bar{x}$	σ	r	p	$\bar{x}$	σ	r	p	$\bar{x}$	σ	r	p
AWS1	-20.44	3.24	-	-	3.38	1.55	-	-	-17.87	31.70	-	-
C05-ref	-20.49	1.95	0.80	0.83	3.41	1.57	0.75	0.83	-30.21	26.01	0.79	< 0.01*
C05-10/0	-20.52	1.92	0.79	0.73	3.48	1.58	0.75	0.48	-30.36	26.22	0.81	< 0.01*
C05-50/1	-20.53	1.92	0.79	0.68	3.46	1.59	0.75	0.56	-29.90	26.35	0.80	< 0.01*
AWS2	-19.50	3.50	-	-	2.63	1.33	-	-	-10.37	37.23	-	-
C05-ref	-20.40	2.23	0.80	< 0.01*	3.33	1.31	0.69	< 0.01*	-28.61	24.32	0.73	< 0.01*
C05-10/0	-20.47	2.13	0.78	< 0.01*	3.36	1.36	0.68	< 0.01*	-28.70	25.33	0.75	< 0.01*
C05-50/1	-20.49	2.13	0.78	< 0.01*	3.36	1.35	0.69	< 0.01*	-28.54	25.13	0.75	< 0.01*
AWS3	-18.91	5.57	-	-	2.75	1.58	-	-	-11.76	30.28	-	-
C05-ref	-19.38	3.07	0.85	0.20	3.17	1.48	0.70	< 0.01*	-24.20	27.34	0.67	< 0.01*
C05-10/0	-19.44	3.10	0.87	0.15	3.17	1.46	0.69	< 0.01*	-23.39	28.95	0.69	< 0.01*
C05-50/1	-19.48	3.08	0.86	0.12	3.17	1.46	0.70	< 0.01*	-23.46	28.93	0.70	< 0.01*
AWS4	-13.36	2.29	-	-	4.17	1.99	-	-	-13.80	26.17	-	-
C05-ref	-16.17	3.29	0.67	< 0.01*	4.67	2.36	0.91	0.12	-35.55	27.63	0.70	< 0.01*
C05-10/0	-16.22	3.25	0.66	< 0.01*	4.75	2.40	0.91	0.07	-34.26	28.51	0.74	< 0.01*
C05-50/1	-16.24	3.28	0.65	< 0.01*	4.65	2.29	0.92	0.13	-34.25	28.51	0.73	< 0.01*

(Riggs et al., 2006). Therefore the number of useful swaths per day is variable. For instance, in the Laptev Sea there are about 10 to 14 swaths per day (2002/03 to 2014/15 (Nov.-Mar.)).

Cloud-induced gaps in our daily sea-ice surface temperature and thin-ice thickness composites were filled by a spatial feature reconstruction procedure (Paul et al., 2015; Preußer et al., 2015a). This method interpolates information of previous and subsequent days to fill gaps caused by cloud-cover. Based on these corrected composites and using the method described in Preußer et al. (2015b), ice production rates were calculated for each pixel with an ice thickness $\leq 0.2\,\mathrm{m}$, i.e. for polynya areas.

In a sensitivity analysis of this method (without the spatial feature reconstruction), Adams et al. (2013) stated an uncertainty for the ice-thickness retrieval of $\pm 1.0\,\mathrm{cm}$, $\pm 2.1\,\mathrm{cm}$ and $\pm 5.3\,\mathrm{cm}$ for thin-ice classes of $0 - 5\,\mathrm{cm}$, $5 - 10\,\mathrm{cm}$ and $10 - 20\,\mathrm{cm}$,

respectively. Therefore, we constrained our analysis to ice thicknesses $\leq 0.2\,\mathrm{m}$, as this range is regarded as sufficient to get reliable results for ice production (Yu and Rothrock, 1996; Adams et al., 2013).

Furthermore, we compared our results to the estimations of Willmes et al. (2011). In their study they used a constant transfer coefficient for heat $C_H = 3 \times 10^{-3}$ to calculate H and E from AMSR-E data and using MODIS thin-ice distributions and National Centers for Environmental Prediction/National Center for Atmospheric Research (NCEP/NCAR) reanalysis data ($2.5° \times 2.5°$) as atmospheric forcing for an energy balance model. However, we omitted the most western polynya mask of their study and compared the IP only to the four remaining masks shown in Fig. 1 and Fig. 2.

We also compared our IP estimations to model-based estimations of Bauer et al. (2013). Bauer et al. (2013) conducted two COSMO simulations at $5\,\mathrm{km}$ horizontal resolution (without a tile-approach) for the same winter 2007/08 in the Laptev Sea. One simulation assumed a grid-scale thin-ice thickness of $10\,\mathrm{cm}$ within polynyas (B10) and one simulation assumed open-water (B00). Both simulations further assumed a sea-ice thickness of $1\,\mathrm{m}$ outside polynyas. Both simulations were forced by a $15\,\mathrm{km}$ COSMO simulation, which was nested within the output of the global GME model.

4 Evaluation with in situ data

The model output of the reference and the five sensitivity simulations were first evaluated with in situ data. During the Transdrift XIII-2 expedition from 11 April to 29 April 2008 four automatic weather stations (AWS, Tab. 2) were deployed on the fast ice of the western New Siberian Polynya (WNS, see Fig 2) (Heinemann et al., 2009). The AWS measured wind speed and direction at $3\,\mathrm{m}$ height with an accuracy of $2\,\%$ in speed and $3°$ in direction; air temperature and relative humidity at $2\,\mathrm{m}$ height with and accuracy of $0.5\,\mathrm{K}$ and $4\,\%$, and pressure with an accuracy of $1\,\mathrm{hPa}$. Furthermore, net radiation was measured by a net radiometer with an accuracy of $5\,\mathrm{W\,m^{-2}}$.

Here, we compared hourly C05 data with the AWS data. In order to judge whether the simulations deviate significantly from the AWS data two-sided t-tests were performed ($\alpha = 95\,\%$). The statistical comparisons were only performed for data pairs without missing values and only for days when the SIC was $> 95\,\%$. This limitation is necessary because the time series of CCLM represent spatial averages of a grid box, whereas the AWS time series are point data on a solid ice cover. If the SIC of CCLM is $< 100\,\%$ then the grid average automatically differs from the station time series, which always represent conditions at $100\,\%$ SIC.

Tab. 3 shows the results for the reference simulation (C05-ref) and two sensitivity simulations: C05-10/0 (subgrid-scale open-water) and C05-50/1 (realistic assumptions). In the remainder of the manuscript, we concentrate on the comparison of these three simulations. Since the comparison was made only over a solid sea-ice cover, the other simulations showed very similar results (not shown).

In general, the inter-model differences are minor for all variables. The comparison for the $2\,\mathrm{m}$ temperature shows that the C05 simulations are generally able to reproduce the observed temperatures during the measurement period. The temporal correlation is about $r = 0.8$, except for the comparison with AWS4. The bias is about $-1°\mathrm{C}$ for AWS2-3, less for AWS1 and about $-3°\mathrm{C}$ for AWS4. Except for the latter, C05 underestimates the variability of the $2\,\mathrm{m}$ temperature. This might be caused

by the assumptions made on snow properties in C05. Although the t-tests are significant for differences of about $1\,°C$, this difference is sufficient for our analysis keeping in mind that grid box averages were compared with point data.

In case of wind speed there is a good agreement ($r \geq 0.7$), although we compared $10\,m$ wind speed of CCLM with measurements at $3\,m$ height. The mean and standard variance are both in accordance with the AWS data, although significant for differences $\geq 0.4\,m\,s^{-1}$. Inversely, this agreement implies that CCLM underestimates wind speeds at $10\,m$, although we do not have reference data at $10\,m$ for a evaluation. Significant differences were found for the comparison of the net radiation. Although the temporal correlation is high ($r \geq 0.7$), the mean of C05 is about $13 - 22\,W\,m^{-2}$ lower than observed meaning a slightly too high heat flux through the sea ice cover. This difference might be caused by the assumption on the sea-ice properties (e.g. a constant temperature at the ice-ocean interface) or by the slight cold bias of the ABL above the sea ice.

Albeit some deviations CCLM is able to reproduce the basic conditions of the near-surface variables during this period with our chosen configurations. However, the reasons for these deviations need further investigation with longer time series.

5   Effects of the tile-approach on the atmospheric boundary layer

5.1   Case study on 4 January 2008

The effects of the TA are exemplified for a case study on 4 January 2008. On this day a low was located over the Taimyr peninsula in the western Laptev Sea. The large pressure gradient generated strong, prevailing off-shore winds, which caused a large opening of polynyas at the fast-ice edge in the Laptev Sea (Fig. 6). The 10 m wind speed reached 10 to $15\,m\,s^{-1}$ and was blowing offshore over the Anabar-Lena polynya (AL). The associated sea-ice concentrations for that day are shown in Fig. 2. Within polynyas, the SIC is between $0\,\%$ and $70\,\%$.

5.1.1   Surface temperature

The surface temperatures (T_{sfc}) of the C05 simulations at 15 UTC (Fig. 6) show a clear signal of the polynyas. Within the AL polynya the surface temperatures are $-22\,°C$ to $-24\,°C$ in C05-ref (Fig. 6a), which is $+6$ to $+16\,°C$ warmer than the surrounding fast and pack ice.

Furthermore, T_{sfc} is about $+2\,°C$ warmer at the downwind side than at the windward side. This is, however, not realistic compared to nature. One would expect higher temperatures at the windward side due to the spatial gradient of the thin-ice with the thinnest or even open water at the windward side. Since in C05-ref a homogeneous thin-ice thickness of $10\,cm$ is assumed within the polynya, this effect is not represented in the simulation.

Much higher surface temperatures were simulated by all sensitivity simulations. As an upper limit, C05-10/0 simulates $> 10\,°C$ higher surface temperatures. This increase of surface temperature is in accordance with results of Bromwich et al. (2009), who found an increase of $14\,°C$ for sea-ice concentrations of about $60\,\%$ in winter. In the more realistic configuration of C05-50/1 temperatures are about $\leq 10\,°C$ warmer. The warmest areas within the polynya tend to be at the windward side now, which is owed to the TA and the thereby considered spatial thin-ice gradient. Another effect, which becomes visible, is
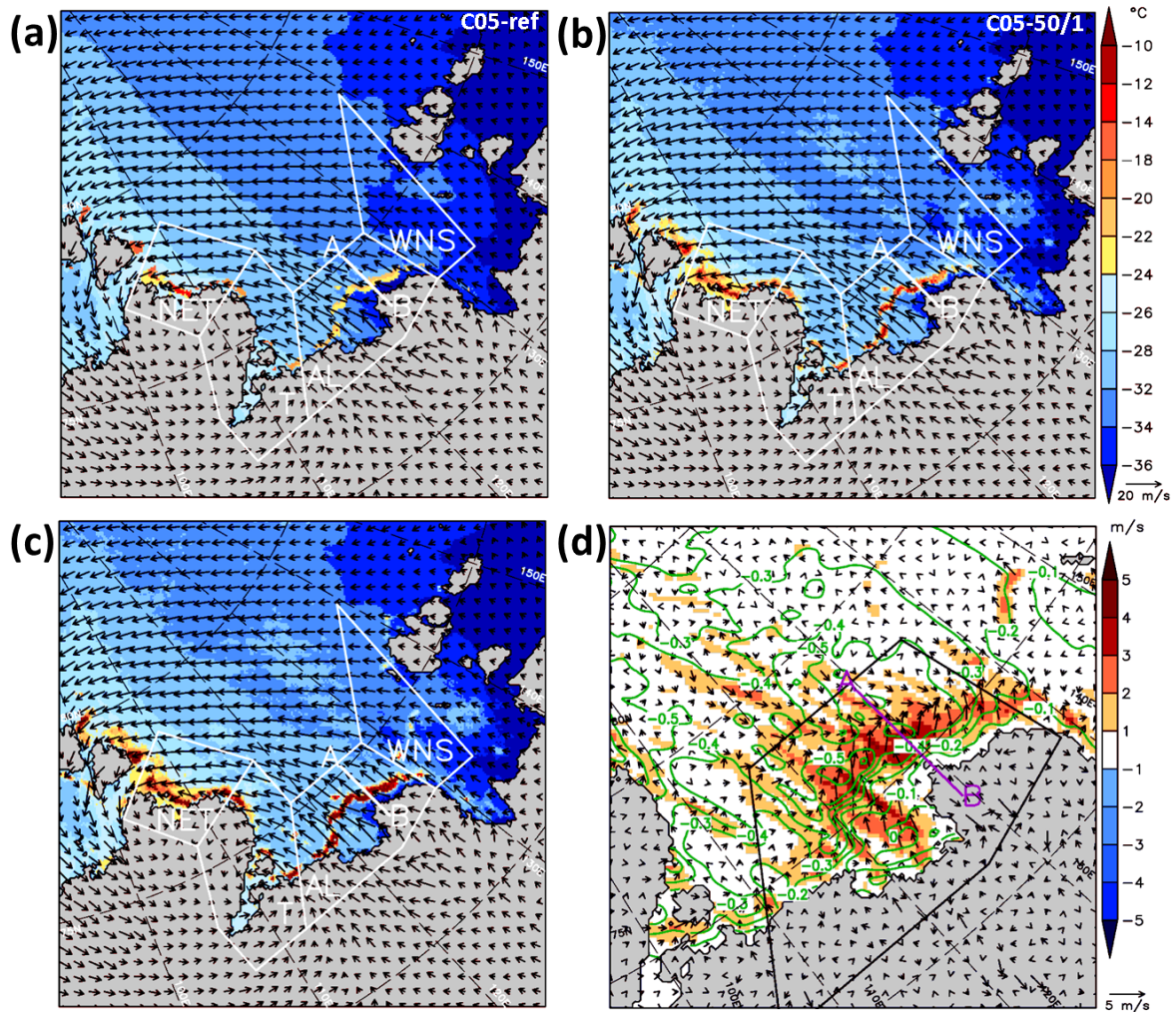
Figure 6. Surface temperature and 10 m wind field on 4 January 2008 at 15 UTC in (a) C05-ref (reference), (b) C05-50/1 (realistic), and (c) C05-10/0 (open-water). In (d) anomalies (C05-10/0 minus C05-ref) over the AL polynya are shown for wind vectors (note different scale) and wind magnitude (colour shaded) at 10 m height and for pressure at mean sea level (green contour lines). The white line in (a) to (c) (magenta in (d)) marks the cross-section A→B used for Fig. 7.

that the marginal area of the polynyas with warmer T_{sfc} increases with the use of TA. This effect is most obvious for the NET polynyas. This increases the area where heat is transferred from the ocean into the atmosphere and causes smooth transitions from the fast or pack ice to the polynyas. An increased heat loss has to be balanced by an increase in frazil ice production.
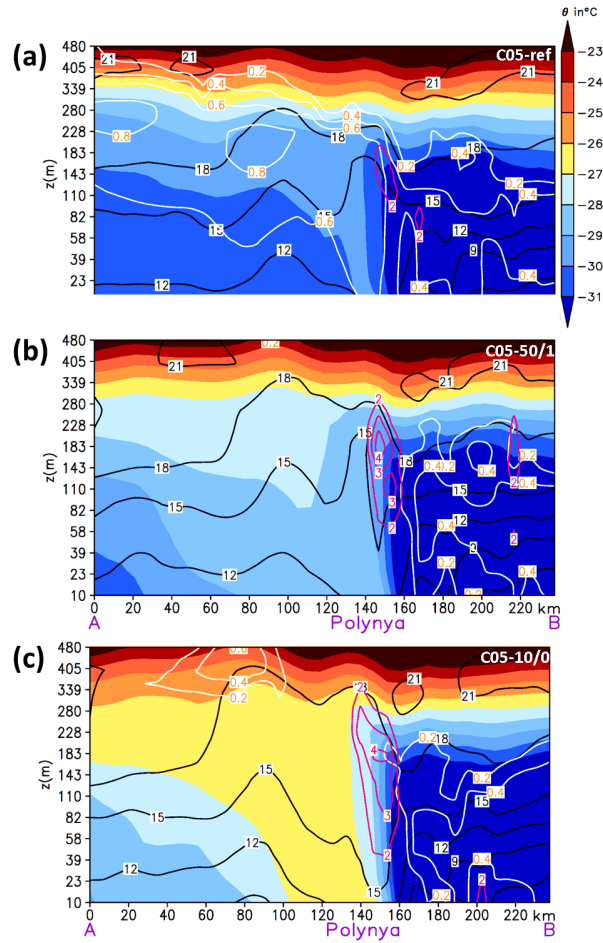
Figure 7. Vertical cross-sections of the potential temperature Θ, horizontal wind speed (black contour lines), turbulent kinetic energy (TKE in $m^2 s^{-2}$, magenta contour lines), and cloud fraction (white contour lines and orange labels) on 4 January 2008 at 15 UTC for (a) C05-ref (reference), (b) C05-50/1 (realistic), and (c) C05-10/0 (open-water). The horizontal distance is about 240 km and the location of the cross-section A (pack ice) → B (fast ice) is shown in Fig. 2.

5.1.2   10 m wind speed

The wind speed is the main driver for mixing in the ABL above polynyas and mainly controls the sensible heat flux until the warming of the ABL reduces the vertical temperature gradient and thus the sensible heat loss and subsequently the ice production. Fig. 6 shows the 10 m wind speed and direction on 4 January 2008 at 15 UTC. In the reference run (C05-ref) the wind speed above the AL polynya is about 14 to $18 \, \mathrm{m \, s^{-1}}$. The wind speed slightly increases (Fig. 6d) in the sensitivity simulations ($+2$ to $+5 \, \mathrm{m \, s^{-1}}$). This increase is caused by increased pressure gradients in the vicinity of the AL polnya which develop as
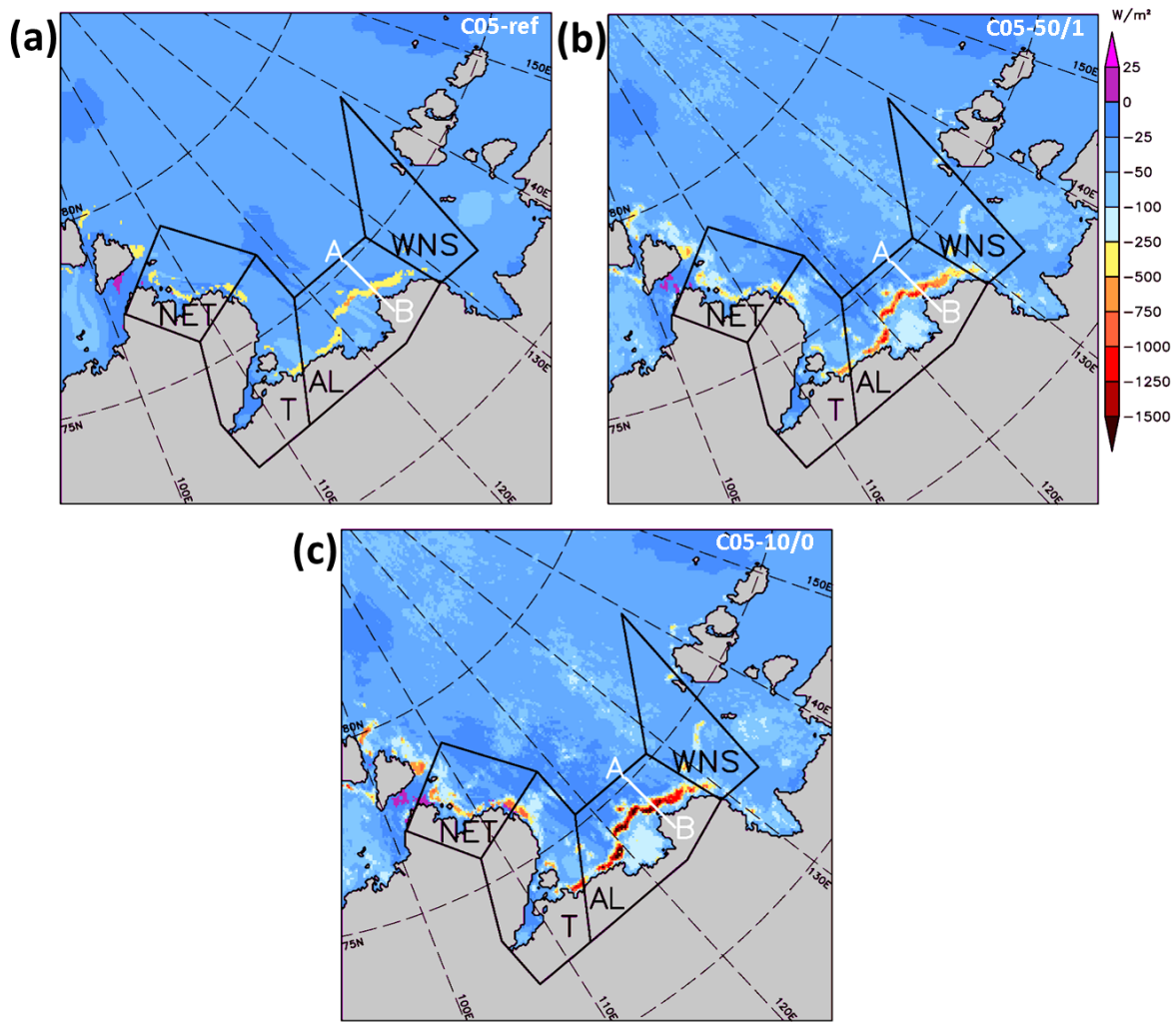
Figure 8. Total atmospheric energy flux on 4 January 2008 at 15 UTC in (a) C05-ref (reference), (b) C05-50/1 (realistic), and (c) C05-10/0 (open-water). Negative fluxes are directed upwards. The white line marks the cross-section A→B used for Fig. 7.

the convection above the polynya lowers the local surface pressure by up to -0.5 hPa. Furthermore, the pressure anomaly is orientaded alongside the polynya resulting in slightly more anticyclonal wind directions. This increase of near-surface wind speed is in aggrement with results from idealized studies conducted by Ebner et al. (2011) (see Fig 5c therein). Ebner et al. (2011) concluded that the increase in wind speed results in an increased net ice production, despite an increased boundary layer warming. The increase in near-surface wind speed causes a larger momentum flux (not shown, but see section 5.1.3 for the turbulent kinetic energy (TKE)) and higher energy loss from the ocean. Furthermore, although not represented in the present CCLM model, higher wind speeds increase the sea-ice drift within polynyas, so that newly formed ice is likely to drift
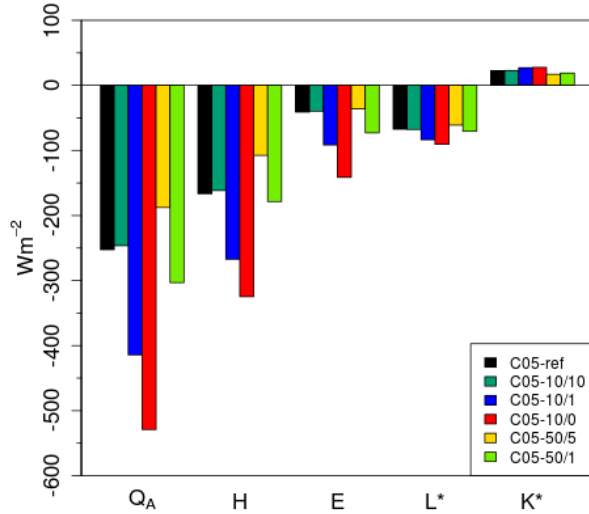
Figure 9. Temporal means of the energy balance Q_A and its components (H: sensible heat flux, E: latent heat flux, L^*: net longwave and K^* net shortwave radiation) averaged over polynya grid boxes for the winter period 2007/08. For the averaging at least 9 grid boxes in the model domain had to be polynyas to include them in the calculation.

faster, so that a strong heat loss is maintained. Both processes are expected to increase the IP. However, the latter issue has to be investigated by coupled atmosphere/sea-ice/ocean model simulations.

5.1.3 Vertical cross-sections

Fig. 7 shows vertical cross-sections of the potential temperature Θ, the horizontal and vertical wind speed, the cloud area
5   fraction and the turbulent kinetic energy (TKE) over the AL polynya. In C05-ref (Fig. 7a) Θ is about $-29\,°C$ at $10\,m$ height over the polynya, about $-30\,°C$ about the pack ice, and colder than $-31\,°C$ over the fast ice. The boundary layer is stably stratified over the pack and the fast ice but over the polynya a well-mixed convective boundary layer (CBL) has developed, capped by an inversion at approximately 300 to $500\,m$ height. Comparing the cross-sections for the three shown model configurations, it becomes obvious that the assumptions on the thin-ice within a polynya has considerable effects on the ABL.

10   As mentioned earlier, the onset of the CBL at the windward polynya edge is displaced to the polynya interior in the reference simulation (C05-ref) compared to the sensitivity simulations. This is owed to the too thick ice in this area, preventing a large enough heat transfer and hence vertical mixing. This is also reflected in the low values of TKE compared to twice as high values for the sensitivity runs. In the open-water configuration (C05-10/0) the CBL is thus about $3\,°C$ warmer than in the reference

run. The warm air spreads as a plume downstream the polynya and can be tracked several hundred kilometres over the pack ice (not shown).

One might suspect that the warmer CBL of the sensitivity simulations might lead to a reduced vertical temperature gradient over the polynya and thus to a negative feedback for the surface sensible heat flux and thus ice production. This is not the case, since the surface temperature in areas with fractional ice cover is also warmer by about $6\,^\circ\mathrm{C}$ to $16\,^\circ\mathrm{C}$, so that the vertical gradient remains or even increases. Secondly, the wind speed in the sensitivity runs is increased over the polynya due to increased local pressure gradients and thus enhances the turbulent fluxes. The increased sensible heat flux causes also TKE production by buoyancy.

Almost all sensitivity simulations show considerably less cloud-formation above and downstream the polynya compared to the reference simulation. Although the amount and location of clouds vary, the clouds almost vanish. The reason for this is that the maximum value of the specific humidity is about $0.4 \times 10^{-3}\,\mathrm{kg/kg}$ over the AL polynya in all simulations and if the CBL warms, the condensation of water vapour is inhibited. As a result, nearly no clouds form above the polynya.

5.1.4 Total atmospheric energy flux

The above mentioned findings result in an increased heat loss from the ocean, which is confirmed and shown in Fig. 8. In the reference simulation the total atmospheric heat flux (Q_A) is, almost homogeneously, about $-500\,\mathrm{W\,m^{-2}}$ over the AL polynya (note that the negative sign denotes upward fluxes). By assuming subgrid-scale open-water the heat loss considerably increases, exceeding $-1000\,\mathrm{W\,m^{-2}}$ at the windward edge and in the center of the polynya. Higher and more structured values of Q_A resulted also from C05-50/1. The smooth transition at the polynya margins is also visible from this figure. Since we based the estimation of ice production on this quantity it is clear that there will be considerable differences as well.

5.2 Energy balance components for the winter period 2007/08

In this section we analyse how the assumptions on subgrid-scale thin ice within the tile-approach affects the energy balance at the surface over the whole winter season 2007/08. We compared daily means of the components of total atmospheric heat fluxes, which were spatially averaged over polynyas (Fig. 9). Thereby, at least 9 grid boxes within the polynya masks have to had a SIC $\leq 70\,\%$ in order to be considered in the analysis.

In principle, the processes presented in section 5.1 come into effect whenever a polynya is present. Thus, if the tile-approach is used Q_A is always more negative due to the consideration of subgrid-scale energy fluxes (Fig. 9) and more energy or heat is lost from the ocean. In the reference simulation (C05-ref) about $-253\,\mathrm{W\,m^{-2}}$ are lost on average within polynyas. If the subgrid-scale thin-ice is reduced or replaced by open-water, than Q_A is much higher, reaching about $-529\,\mathrm{W\,m^{-2}}$ in the latter, which is about $+110\,\%$. In the simulation with a realistic configuration (C05-50/1) the increase is about $+20\,\%$ reaching about $-303\,\mathrm{W\,m^{-2}}$ on average.

The largest contribution to Q_A constitutes the sensible heat flux H (Fig. 9). About $66\,\%$ of the heat is lost via H in the reference simulation, which slightly decreases to $57\,\%$ to $65.6\,\%$, if the tile-approach is used. The strongest impact on the
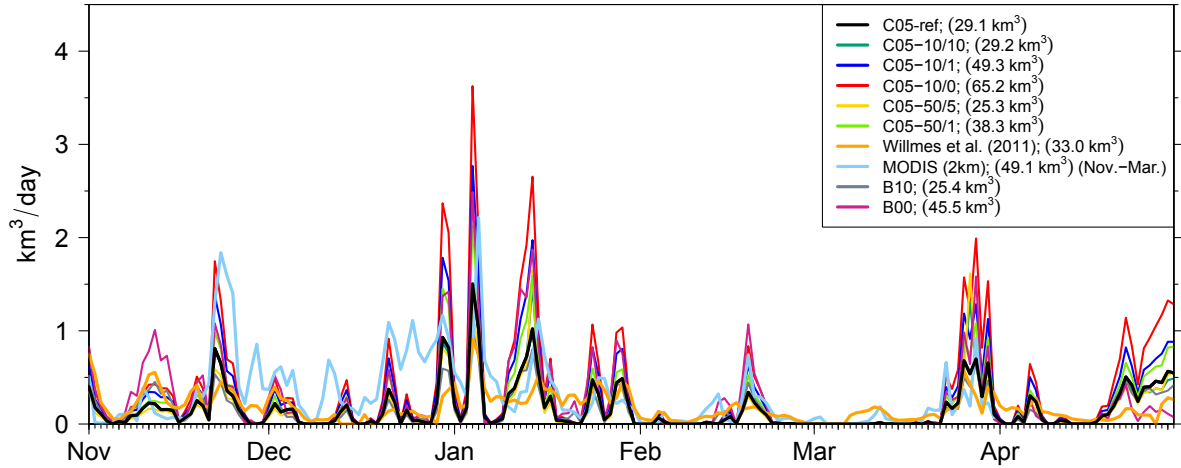
Figure 10. Daily sea-ice production within the Laptev Sea polynyas in the winter period 2007/08, aggregated within the four polynya masks (only considering polynyas $> 277\,\mathrm{km}^2$ in the C05 and Bauer et al. (2013) simulations (B10, B00)). The total sea-ice production is given in parenthesis in the legend (see also Tab. 4).

sensible heat flux shows C05-10/0. Here, H doubles from $167\,\mathrm{W\,m}^{-2}$ in C05-ref to $-325\,\mathrm{W\,m}^{-2}$ due to the absence of the isolating sea-ice cover. The increase is less in the other sensitivity simulations, e.g. $+7.1\,\%$ in case of C05-50/1.

The other components contribute much less to the heat loss. However, the Bowen ratio (Bowen, 1926), which is the ratio H/E, reduces from about 4.0 (C05-ref) to 2.5 (C05-50/1) and 2.3 (C05-10/0). The latent heat flux (E) nearly doubles for C05-50/1 compared to C05-ref, which is caused on one hand by the increase of the vertical gradient of specific humidity and on the other hand by the increase of the near-surface wind speed and TKE, enhancing the turbulence above the polynyas. Shortwave radiation K^* only becomes important in the time from March until April, when the melting season begins. Therefore, K^* is small compared to the other terms.

6   Effects on sea-ice production in the winter period 2007/08

The daily sea-ice production rates were calculated for the individual polynyas as described in section 3.4. Here we compared the ice production of the C05 simulations to the remote sensing estimations of Willmes et al. (2011), to estimates based on MODIS2km (section 3.4), and to model results of Bauer et al. (2013).

The time-series of daily IP ($\mathrm{km}^3/\mathrm{day}$) are shown in Fig. 10 and the total ice production for the whole winter are shown in Tab. 4. The total IP in the winter 2007/08 is about $29.1\,\mathrm{km}^3$ in the reference simulation (C05-ref), which is not significantly

Table 4. Total sea-ice production (IP) (km^3) in the winter period 2007/08, aggregated over polynyas within the four polynya masks (Fig. 2). The daily mean $(\bar{x})$ and standard deviation (σ) are given in km^3/day. The Pearson correlation coefficient (r) was calculated with the IP time series and the estimates of Willmes et al. (2011). The 95% confidence interval (CI) of r was calculated based on the Fisher z-transformation. The critical value is $r_{c,\alpha=0.05,n=182} = 0.15$ and r is significant if $r > r_c$. Two-sided t-tests $(\alpha = 5\%)$ were performed and the resulting p-values (p) values are given. Significant differences are marked with *. The results from Bauer et al. (2013) assumed an ice thickness of $10\,\text{cm}$ (B10) or open-water (B00) within polynyas, both without a tile-approach.

Data	total	$\bar{x}$	σ	r [95 % CI]	p
C05-ref	29.1	0.2	0.2	0.65 [0.56;0.73]	0.30
C05-10/10	29.2	0.2	0.3	0.63 [0.53;0.71]	0.34
C05-10/1	49.3	0.3	0.4	0.63 [0.53;0.71]	0.01*
C05-10/0	65.2	0.4	0.6	0.61 [0.51;0.69]	< 0.01*
C05-50/5	25.3	0.1	0.3	0.56 [0.45;0.65]	0.05*
C05-50/1	38.3	0.2	0.3	0.60 [0.50;0.69]	0.30
Willmes et al.	33.0	0.2	0.2	-	-
MODIS2km[1]	49.1[1]	0.3[1]	0.4[1]	0.45 [0.33;0.56][2]	< 0.01*[2]
B10	25.4	0.1	0.2	0.67 [0.58;0.74]	0.02*
B00	45.5	0.3	0.4	0.68 [0.59;0.75]	0.03*

[1] Only for November - March.

[2] Comparisons with Willmes et al. (2011) were made only for November - March.

different from the $33.0\,\text{km}^3$ estimated by Willmes et al. (2011). The temporal correlation is $r = 0.65$, which is sufficiently high, but some differences are visible (Fig. 10). This result agrees well with the remote sensing estimates, although Willmes et al. (2011) used a constant C_H for calculating the heat fluxes and much coarser atmospheric data.

The strongest, significant increase $(p < 0.01)$ in IP was estimated from C05-10/0 with $65.2\,\text{km}^3$ $(+125\%)$, where subgrid-scale open-water was assumed. For realistic assumptions (C05-50/1) the IP increases to $38.3\,\text{km}^3$ $(+39\%)$, which is not significant at the 95 % level. The increase of IP is caused by the higher heat fluxes from the ocean into the overlying atmosphere as presented above. Compared to the results based on MODIS2km, where we estimated about $49.1\,\text{km}^3$ due to the large polynya area, most of the simulations produced much less ice. Exceptions are C05-10/0 and C05-10/1, which reach or even exceed this estimate. These results show that there are large differences not only between the models but also between remote sensing approaches. For instance, also the time of polynya openings and IP differ $(r = 0.45)$. Although such high IP could be reproduced in the Laptev Sea, the question remains which remote sensing data set should be used for calibrating the models.

The IP based on an older reference COSMO simulation by Bauer et al. (2013) with $10\,\text{cm}$ ice within polynyas (B10) is slightly less compared to our reference run (C05-ref), but significantly lower compared to Willmes et al. (2011). Although the open-water sensitivity run of Bauer et al. (2013) (B00) produces higher IP, it is considerably less compared to our C05-10/0 run. B10 and B00 show a slightly higher correlation with the IP time series of Willmes et al. (2011). The differences of B10/B00 with respect to our C05 simulations can be explained by differences in the model version, configuration, and nesting chain (GME vs. ERA-Interim, different model domains). However, we cannot quantify the individual contributions to the deviations.
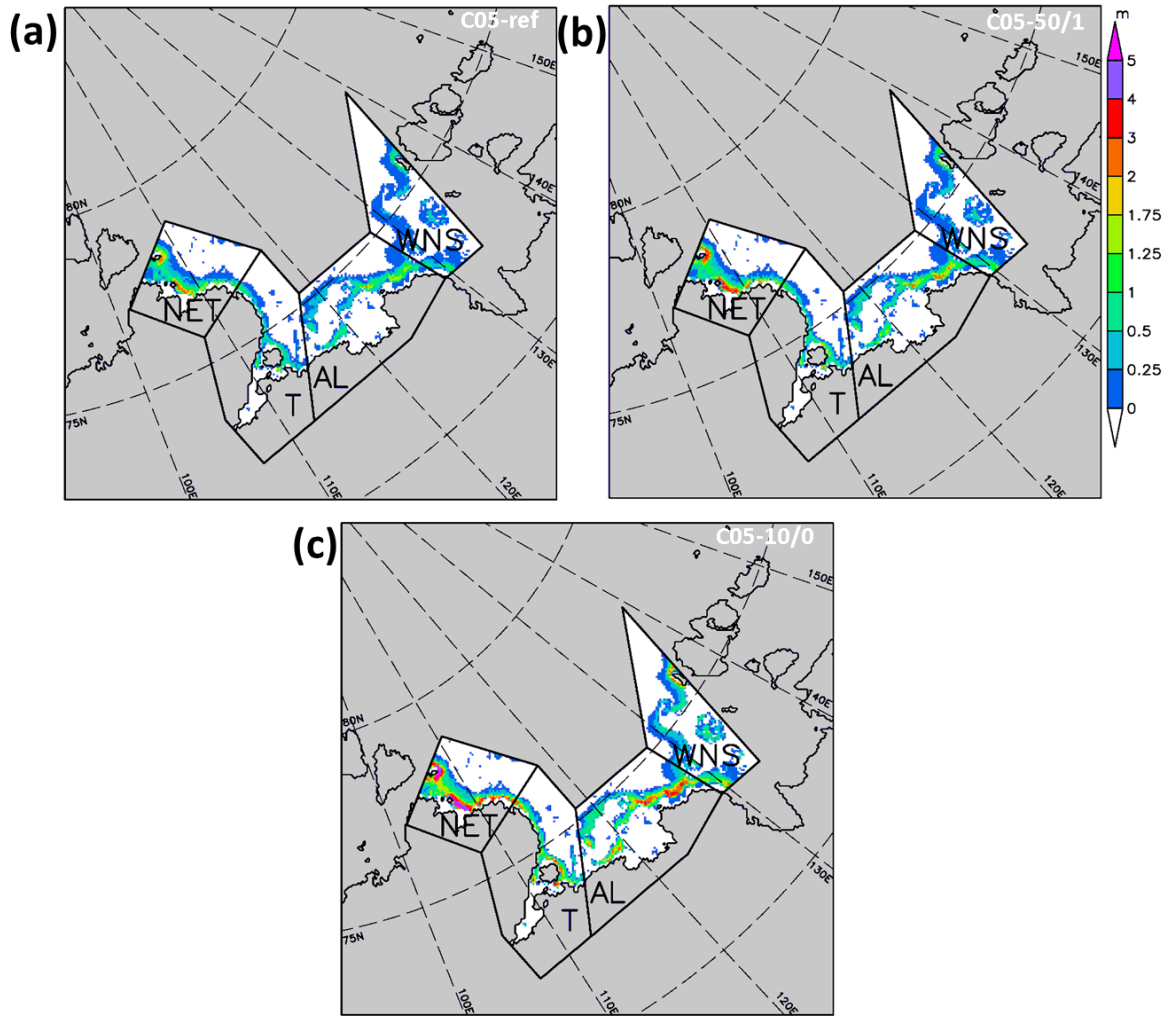
Figure 11. Total sea-ice production (m) within the Laptev Sea polynyas in the winter period 2007/08 simulated by (a) C05-ref (reference), (b) C05-50/1 (realistic), and (c) C05-10/0 (open-water).

All C05 sensitivity simulations show a higher daily standard deviation compared to the data from Willmes et al. (2011), which increases with decreasing subgrid-scale thin-ice. This is logical since if a polynya opens more heat is released compared to the reference simulation and thus the IP is higher.

Spatial maps of the total IP within polynyas in the winter 2007/08 are shown in Fig. 11. In all simulations the highest IP occurs in the NET polynyas, with rates $> 2\,\mathrm{m}$/winter in C05-ref and $> 5\,\mathrm{m}$/winter in C05-10/0. Further, with considering the subgrid-scale thin-ice or open-water the spatial gradient of ice production is much better represented, with higher rates at the windward edge of the polynyas. Overall, we think that the assumptions made in C05-50/1 are realistic. Although we are aware
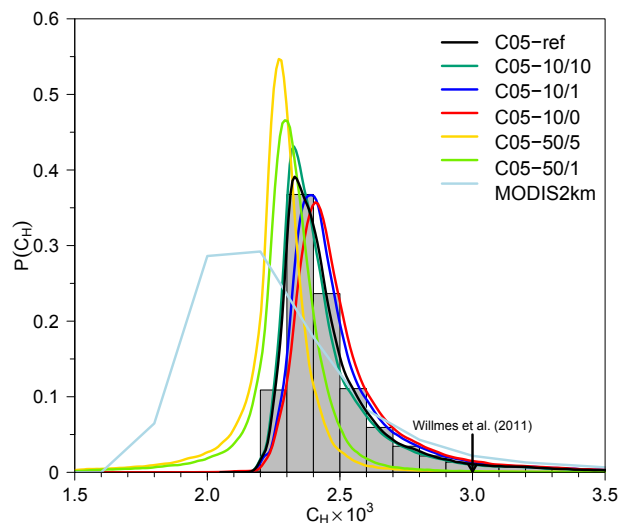
Figure 12. Probability density functions of the turbulent transfer coefficients for heat (C_H) within the Laptev Sea polynyas in the winter period (Nov.-Apr.) 2007/08, aggregated within the four polynya masks. The grey bars show the histogram of C_H from C05-ref. Only values below $6 \cdot 10^{-3}$ have been used for the construction of this figure. The mean values of the C05 simulations are $\approx 2.5 \cdot 10^{-3}$ and the standard deviations are $\approx 0.28 \cdot 10^{-3}$, except for C05-50/5 and C05-50/1 where the mean values are $\approx 2.27 \cdot 10^{-3}$ and $\approx 2.31 \cdot 10^{-3}$, and the standard deviations are $\approx 0.18 \cdot 10^{-3}$, respectively. The constant value of $C_H = 3.0 \cdot 10^{-3}$ of Willmes et al. (2011) is marked with an arrow. The mean C_H value derived from MODIS2km (Nov-Mar.) is $C_H = 2.3 \pm 0.3 \cdot 10^{-3}$.

that open-water areas may occur at the windward site of polynyas, the area of open-water is much smaller compared to the entire polynya area (see Fig. 3). Thus, the heat flux and IP would be overestimated if open-water is assumed in every grid box with fractional sea ice.

7 Discussion

5   The simulation results of our study showed that there is a high sensitivity of the ice production to the assumptions on subgrid-scale thin-ice distribution, with considerable effects on the atmospheric boundary layer. The ABL receives more heat the thinner the ice is and warmed by up to $+3\,°C$ in our subgrid-scale open-water configuration. However, the warmer ABL did not prevent further heat release from the ocean due to a weakened vertical temperature gradient. The simulations showed that the vertical temperature gradients remain or even exceed the gradients of the reference simulations. Two effects are responsible

10   for this: (i) as the ice becomes thinner the surface temperature increases stronger than the heating of the ABL, which increases the vertical gradient, and (ii) the near-surface wind speed is enhanced due to increased local pressure gradients, which increases the wind-shear and thus the sensible heat fluxes. Further, the warm plumes over the polynyas are efficiently advected over the

pack ice. Thus heat is removed from above the polynyas and a strong temperature gradient is maintained, which enhances the ice production.

Constraining the assumptions on subgrid-scale thin-ice was found to be difficult. The comparison of model-based IP with remote sensing estimates revealed large discrepancies. Further, large differences were found between the two remote sensing approaches. The usage of higher resolved MODIS data and ERA-Interim, compared to the approach of Willmes et al. (2011), where NCEP and AMSR-E data were used, nearly produced $+50\%$ more ice. The configuration of C05-50/1, where we assumed 50 cm thick grid-scale and 1 cm subgrid-scale thin-ice, seems to be a realistic assumption in the marginal ice zone of the polynyas.

The resulting IP is close to the estimates of Willmes et al. (2011), which we defined as a baseline for our sensitivity experiment. However, if for instance the results of MODIS2km would be defined as a baseline, then even thinner ice might be considered. We are aware that our sea-ice module is simplified compared to more sophisticated sea-ice models, where the thin-ice thickness might be a prognostic variable and not a constant. However, despite our simple assumption, the results are promising and satisfactory in order to represent sea ice in a regional climate model in a computationally cheap approach. We further argue, based on our results, that assuming subgrid-scale open-water within fractional sea ice, such as in Polar-WRF (Bromwich et al., 2009) leads to too high heat fluxes from the ocean into the atmosphere.

However, even if more sophisticated sea-ice models were used to estimate the IP, the issues of how to constrain parameters and to which data set to compare with remain. It is not our intention to entangle all factors controlling the estimation of sea-ice production based on different approaches, data sets or models, but several issues are important in a general sense:

- Polynya area is affected by the definition of polynyas (e.g. SIC $\leq 70\%$ or $h_i < 0.2\,\mathrm{m}$) and the horizontal resolution of the model and the satellite products.

- Heat loss is affected by the vertical temperature gradient, wind speed, parameterization of the energy balance components (turbulent fluxes), sea-ice thickness and properties, and by the parameterization of the heat flux through the ice. Particularly important is the horizontal resolution of the atmospheric data set and the assumptions on the turbulent exchange coefficient for heat (C_H). Willmes et al. (2011) assumed a constant value of $C_H = 3 \cdot 10^{-3}$. However, the mean values from C05 over polynyas (winter 2007/08) are about $(2.5 \pm 0.28) \cdot 10^{-3}$ (Fig. 12), except for C05-50/5 and C05-50/1, which simulated slightly lower values of $(2.27 \pm 0.18) \cdot 10^{-3}$ and $(2.31 \pm 0.18) \cdot 10^{-3}$.

- Since the warm surface temperatures of polynyas and the resulting vertical temperature gradients are not well represented in ERA-Interim or NCEP, the usage of a high value of C_H seems to partly compensate for this issue. The C_H values based on MODIS data and ERA-Interim are lower than simulated by CCLM with a mean of $C_H = (2.3 \pm 0.3) \cdot 10^{-3}$. A similar probability distribution function was derived by Adams et al. (2013), who combined MODIS and NCEP. Because of the horizontal resolution of MODIS, polynyas are represented as anomalies in the surface temperature field causing larger vertical temperature gradients and hence C_H values, which are comparable to CCLM.

– Surface temperatures in remote sensing approaches also depend on the number of swaths per day, e.g. clear-sky conditions, and their distribution over the day. If not equally distributed, the surface temperature and the ice production may be biased.

These influence factors together control differences between model and remote sensing sea-ice production estimates within polynyas. The polynya area is an obvious factor with the simple relationship: the larger the polynya area the larger the sea-ice production. Note that sea ice growths also outside polynyas, which was simulated by our model and contributed to the total IP. However, compared to the contribution of the polynya areas to the total the IP of such areas is of minor importance. The explanations for differences in the heat or energy loss within polynyas is manifold. In our opinion, the most relevant factors, besides polynya area, are the thin-ice thickness and the parameterizations of the turbulent heat fluxes, in particular the differences in C_H.

The complexity of these factors make a comparison of model and remote sensing studies difficult. It further indicates that some assumptions in the remote sensing approaches, such as a constant value for C_H, might be oversimplified. Furthermore, a problematic issue is the usage of coarse atmospheric data sets, such as NCEP or ERA-Interim, for remote sensing approaches, if not combined with high-resolution satellite products. The horizontal resolution of such atmospheric reanalysis data sets is not sufficient to represent polynyas adequately. Thus subsequent errors, such as wrong simulations of the atmospheric boundary layer over polynyas, are the consequence. These errors are then transferred to the remote sensing approach and might result in wrong sea-ice production estimates. From a modelling point of view the question arises what reference for IP estimates should be used? This question is not easily answered and is still an open issue. A strategy might be a simultaneous application of both, modelling and remote sensing approaches, in order to compensate for weaknesses. This issue directly impedes the decision of an optimal model configuration.

According to our study, the approach of Willmes et al. (2011) constitutes the closest reference because of the same satellite data that were used to derive polynya area at a comparable horizontal resolution. Although the definitions of polynyas are different, the assumption of $0.1\,\mathrm{m}$ thin-ice in areas of SIC $\leq 70\,\%$ is similar to the definition of $\leq 0.2\,\mathrm{m}$ as in Willmes et al. (2011). Larger differences evolve from the assumptions made on C_H (Fig. 12) and the horizontal resolution of the atmospheric data. Given these deviations, the IP based on C05-ref and C05-50/1 are still close to the results of Willmes et al. (2011). Although the use of MODIS, i.e. higher resolved satellite products, results in higher IP estimates, the reason for this is the higher horizontal resolution that causes larger polynya areas and not the representation of subgrid-scale energy fluxes within polynyas in ERA-Interim, which is still too coarse. For thicker ice the C_H values converge to $\leq 1.5 \cdot 10^{-3}$, a value also reported by Schröder et al. (2003).

Given these issues, the decision which TIT should be used with the TA is another degree of freedom and cannot sufficiently be answered from our study. A justified assumption is to rely on MODIS TIT (Fig. 3). The mean derived TIT for the winter periods (Nov.-Mar.) 2002/03–2014/15 is $13.5 \pm 0.5\,\mathrm{cm}$, which is slightly thicker than our assumed TIT in CCLM. Unfortunately, the MODIS TIT distribution for the polynya areas shows no maximum at a specific ice thickness, which gives no preference for the choice of the sub-grid TIT for the tile approach.

8 Conclusions

In this study we quantified the ice production in the Laptev Sea polynyas for the winter 2007/08 based on simulations with a regional atmospheric model (CCLM) and remote sensing data. A new tile approach for fractional sea ice, considering subgrid-scale thin-ice, was implemented into CCLM. Besides a reference run, five sensitivity simulations with different assumptions on grid-scale and subgrid-scale ice within polynyas were performed. We further investigated the impact on the atmospheric boundary layer above polynyas.

The results show that the ice production is highly sensitive to the assumptions made on the ice thickness within polynyas. Compared to the estimated total winter ice production of $29.1\,\mathrm{km}^3$ of the reference simulation, the ice production more than doubled if subgrid-scale open-water was assumed, and increased by about $(+39\%)$ for the most realistic assumptions based on remote sensing of ice thickness. The increase of the ice production is caused by a larger heat loss from the ocean, whose magnitude is proportional to the thin-ice thickness. Although the atmospheric boundary layer is heated by up to $+3\,^\circ\mathrm{C}$ in the open-water configuration, strong vertical temperature gradients and associated high sensible heat fluxes at the surface were maintained. On one side, the tile-approach improves the physical representation of polynyas in CCLM because fractional sea ice is considered, on the other side a new degree of freedom is introduced to constrain the thin-ice thickness. The derivation of an optimal configuration for CCLM or other regional climate models remains difficult because of sparse observed ice thickness distributions within polynyas. We used remote sensing data as a baseline to constrain our configuration, but several issues were found, which hamper such comparisons. At this point coupled atmosphere-ice-ocean models are needed to fully simulate feedback processes.

In summary, realistic ice production estimates could be retrieved from our simulations. Neglecting subgrid-scale energy fluxes might considerably underestimate the ice production in coastal polynyas, such as in the Laptev Sea, with possible consequence on the Arctic sea-ice budget.

Appendix A: Sea-ice albedo scheme

We implemented a modified Køltzow scheme (Køltzow, 2007) (Fig. 13) to replace the default treatment of sea-ice albedo, which was previously set to $\alpha_i = 0.75$ for ice thickness $> 0.1\,\mathrm{m}$ and $\alpha_i = 0.2$ for ice thickness $\leq 0.1\,\mathrm{m}$ (Schröder et al., 2011). Furthermore, the Køltzow scheme includes a parameterization of melt ponds (see Køltzow (2007) for details), yet they are of no importance for our study. The scheme is based on measurements retrieved during the Surface heat Budget of the Arctic Ocean (SHEBA) project (Uttal et al., 2002). It is forced by the surface temperature T_{sfc}, which may be either the ice (T_i) or the snow surface temperature (T_s) (Fig. 4). If no snow cover is present the albedo only depends on the ice thickness. If the ice thickness exceeds the threshold value of $h_c = 0.2\,\mathrm{m}$, a snow cover on sea ice is assumed in accordance to the sea-ice module.
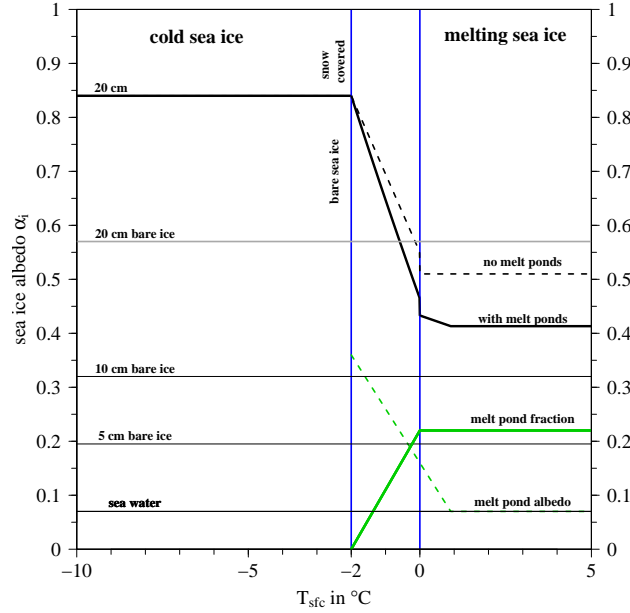
Figure 13. Sea-ice albedo resulting from the modified Køltzow-scheme (Køltzow, 2007) in dependence of the ice surface temperature and thickness. Thereby the threshold thickness above which a snow cover of 10 cm is assumed is $h_c = 0.2\,\mathrm{m}$ (bold black line). In addition the melt pond fraction is shown as a function of the ice temperature (bold green line) and the resulting modification (dashed green line) of the sea-ice albedo (dashed black line). For bare sea-ice (thin black lines) a constant albedo value is assumed, which is linearly decreasing from 0.57 (Persson et al., 2002) at 20 cm ice thickness (bold grey line) to 0.07 (ocean albedo, Perovich and Grenfell (1981)), but constant over all surface temperatures, as shown in Eq. (A2). The vertical blue lines mark the transition range from cold to melting conditions.

Sea ice thicker than h_c is treated as thick ice and the albedo is estimated by:

$$\alpha_i = \begin{cases} 0.84 & \text{if } T_{sfc} \leq -2\,^{\circ}\mathrm{C} \\ 0.84 - 0.145(2 + T_{sfc}) & \text{if } 0\,^{\circ}\mathrm{C} > T_{sfc} > -2\,^{\circ}\mathrm{C} \\ 0.51 & \text{if } T_{sfc} > 0\,^{\circ}\mathrm{C}. \end{cases} \tag{A1}$$

Køltzow (2007) sets the albedo for cold sea ice to a high value of 0.84, which is supposed to include the effects of snow on sea ice in winter and spring. In the original scheme Køltzow (2007) set the threshold for thin ice to $h_c = 0.25\,\mathrm{m}$, but since the values above are only valid for snow covered sea ice, we set $h_c = 0.2\,\mathrm{m}$ to be consistent with the sea-ice module.

For thin-ice, we implemented a linear decrease towards the ocean albedo ($\alpha_o = 0.07$):

$$\alpha_i = \alpha_o + (h_i/h_c) \cdot (\alpha_c - \alpha_o) \tag{A2}$$

As a starting value we use $\alpha_c = 0.57$, the albedo of thick bare sea ice from Persson et al. (2002).

Fig. 13 shows a summary of both cases. If the ice thickness is at least $0.2\,\mathrm{m}$ (bold black line) then the albedo is constant ($\alpha_i = 0.84$) for cold, snow covered sea ice. It decreases with increasing surface temperature, if $-2\,°\mathrm{C}$ are exceeded. This temperature denotes a threshold where melting begins and sea ice is changing its albedo characteristics. In addition, if melt ponds occur (black solid line), the albedo is somewhat lower during the melting season. The fraction of melt ponds increases with $T_{sfc} > -2\,°\mathrm{C}$ to a maximum of $22\,\%$ (bold green line), an upper limit set by Køltzow (2007), and the albedo of melt ponds converges to the albedo of sea water (dashed green line). Furthermore, in Fig. 13 the thin-ice albedo is exemplified for four ice thicknesses which are not covered with snow and for which a constant albedo is assumed (thin black lines).

If the tile-approach is used, subgrid-scale open water reduces the grid-average albedo accordingly, compared to a complete coverage with sea ice. A comparable, though less pronounced, reduction of albedo occurs if 1 cm thin-ice coverage is assumed for subgrid-scale open water.

Appendix B: Implementation of the tile-approach in CCLM

In order to simulate the subgrid-scale energy fluxes over fractional sea ice, it is necessary to differentiate the energy balance and its components over water and ice. Over sea ice (index $k = i$) or ocean (index $k = o$) the total atmospheric heat flux (see Fig. 4) is:

$$Q_{A,k} = K_k^* + L_k^* + H_k + E_k \tag{B1}$$

with K_k^* the net shortwave radiation, L_k^* the net longwave radiation, H_k the turbulent flux of sensible heat and E_k the turbulent flux of latent heat.

All routines of CCLM, except the sea-ice and the turbulence module, calculate with grid-box averaged coefficients or fluxes (flux averaging approach, Vihma (1995)), which is best suited if the sea-ice module only requires the fluxes over ice (Lüpkes and Gryanik, 2014). The procedure is described in section B3.

As initial data the module requires the sea surface temperature (SST), the sea-ice fraction (A) and extent, the sea-ice thickness (SIT), the surface temperature of sea ice (T_i), specific humidity at the ice surface, the wind-speed on the lowest model level, and incoming longwave and shortwave radiation (see Schröder et al. (2011) for more details).

The calculation of the components of the energy balance equations are shown in the next subsections.

B1 Shortwave radiation

The grid-box average of the albedo α_m (index m for 'mixed') is calculated as:

$$\alpha_m = A \cdot \alpha_i + (1 - A) \cdot \alpha_o, \tag{B2}$$

with A the sea-ice fraction, $\alpha_o = 0.07$ the albedo of the ocean, and $\alpha_i = f(T_i, h)$ the albedo of sea ice as a function of sea ice temperature (T_i) and thickness (h) (see section A). Based on this mixed albedo the upward shortwave radiation is calculated

as:

$$K \uparrow_m = \alpha_m \cdot K \downarrow, \tag{B3}$$

with $K \downarrow$ the incoming shortwave radiation. The grid-box average net shortwave radiation is calculated as:

$$K_m^* = K \downarrow - K \uparrow_m = (1 - \alpha_m) \cdot K \downarrow. \tag{B4}$$

5   This grid-box averaged net shortwave radiation is the input for the sea-ice module where the upward shortwave radiation over ice $K \uparrow_i$ is calculated as:

$$K \uparrow_i = \alpha_i \cdot K \downarrow, \tag{B5}$$

The final net shortwave radiation over sea ice or ocean becomes:

$$K_k^* = (1 - \alpha_k) \cdot K \downarrow = \frac{1 - \alpha_k}{1 - \alpha_m} \cdot K_m^* \tag{B6}$$

10   where the index k refers either to i (sea ice) or o (ocean).

B2   Longwave radiation

The subgrid-scale ocean surface temperature (T_o) is assumed to be at the freezing point ($-1.7\,°\mathrm{C}$) if open water is assumed, or to be a prognostic variable if a thin-ice cover is assumed. The ice surface temperature (T_i) is also a prognostic variable in the sea-ice module.

15   To account for subgrid-scale longwave radiation, we calculate the upward longwave radiation over sea ice and ocean as:

$$L \uparrow_k = \epsilon \sigma T_k^4 - (1 - \epsilon) L \downarrow, \tag{B7}$$

with σ the Stefan–Boltzmann constant, $L \downarrow$ the incoming longwave radiation, ϵ the surface emissivities of sea water and ice, which are assumed to be equal ($\epsilon = 0.996$), and T_k the surface temperature of ice or ocean.

Then the net longwave radiation balance over sea ice or ocean becomes:

$$L_k^* = L \downarrow - L \uparrow_k. \tag{B8}$$

B3   Turbulent fluxes of sensible and latent heat

We modified the parameterization of the turbulent fluxes of sensible (H) and latent heat (E) within a grid box, in contrast to the standard version of CCLM and the sea-ice module of Schröder et al. (2011). Over sea ice or ocean the roughness length z_0 and the turbulent coefficients of heat and moisture C_H were previously calculated from the predominant surface type of a grid
25   box: ice or sea water. We modified this procedure by a tile-approach; now the fluxes are calculated both for sea ice and ocean within a grid box with different z_0 and C_H. Afterwards they are averaged in a 'flux-averaging approach' and an average C_H

is calculated for other modules. The calculation of the momentum flux is not modified and for the details of the calculation we refer the reader to Doms et al. (2011).

In CCLM a stability and roughness length dependent surface flux formulation is used, which is based on flux calculations after Louis (1979). The fluxes are calculated with a bulk approach:

$$H = -\rho c_p C_H |v_h| (\Theta_{sfc} - \Theta) \tag{B9}$$

$$E = -\rho L_f C_H |v_h| (q_{sfc} - q) \tag{B10}$$

with ρ the air-density, c_p the heat capacity of air, Θ and Θ_{sfc} the potential temperature at the lowest model layer and at the surface (ice or ocean). q and q_{sfc} are the specific humidity at the lowest model layer and at the surface (ice or ocean), L_f the latent heat of fusion (and sublimation in case of sea ice), $|v_h| = \sqrt{u^2 + v^2}$ the absolute wind speed, and C_H the turbulent transfer coefficient for heat and moisture.

To calculate the turbulent transfer coefficients it is first necessary to calculate the roughness length of sea-water ($z_{0,o}$) and sea ice ($z_{0,i}$). In case of sea ice we set $z_{0,i} = 0.001\,\mathrm{m}$ as in Schröder et al. (2011). Over open water a modified Charnock-formula is used (see Doms et al., 2011). In case of H and E, we assume the additional roughness length for heat z_h (Doms et al., 2011) to be equal to z_0 over subgrid-scale open ocean within the sea-ice cover.

The transfer coefficients are calculated over sea ice ($C_{H,i}$) and ocean ($C_{H,o}$), respectively. The turbulent fluxes over sea ice (H_i, E_i) and ocean (H_o, E_o) can be retrieved by inserting these coefficients into Eqs. (B9-B10). Then all terms of Eq. (B1) are known to solve the energy balance over both surface types.

The fluxes of sensible and latent heat, the turbulent transfer coefficient for heat, and the surface temperature are averaged according to the sea-ice concentration A:

$$H_m = A \cdot H_i + (1 - A) \cdot H_o \tag{B11}$$

$$E_m = A \cdot E_i + (1 - A) \cdot E_o, \tag{B12}$$

$$C_{Hm} = A \cdot C_{H,i} + (1 - A) \cdot C_{H,o}, \tag{B13}$$

$$T_{sfc} = A \cdot T_i + (1 - A) \cdot T_o \tag{B14}$$

The grid averaged temperature fields are used for the comparisons in section 5.

Author contributions. O. Gutjahr implemented the tile-approach and other modifications to the CCLM source code, conducted the CCLM simulations, designed the study and wrote the paper. G. Heinemann assisted in designing the experiments and the structure of the paper, as well as the writing process. A. Preußer wrote the section on MODIS and calculated the sea-ice production from MODIS data, S. Willmes calculated the ice production rates based on AMSR-E and NCEP and assisted in the discussion on the comparison of remote sensing and modelling results. C. Drüe contributed to the translation of the equations into source code.

Acknowledgements. This work was funded by the German Ministry for Education and Research under grant 03G0833D, and is part of the German-Russian Transdrift project. We thank the CLM-Community and the German Meteorological Service for providing the basic COSMO-CLM model. The AMSR-E data was provided by the University of Bremen, the MODIS data were provided by the US National Snow and Ice Data Center, ERA-Interim by the ECMWF, and the PIOMAS data set by the Polar Science Center (University of Washington).

5   Finally, we thank the DKRZ for providing computational time and two anonymous reviewers for critical comments.

References

Aagard, K., Coachman, L., and Carmack, E.: On the halocline of the Arctic Ocean, Deep Sea Res., 28, 529–545, doi:10.1016/0198-0149(81)90115-1, 1981.

Adams, S., Willmes, S., Heinemann, G., Rozman, P., Timmermann, R., and Schröder, D.: Evaluation of simulated sea-ice concentrations from sea-ice/ocean models using satellite data and polynya classification methods, Polar Res., 30, doi:10.3402/polar.v30i0.7124, 2011.

Adams, S., Willmes, S., Schroeder, D., Heinemann, G., Bauer, M., and Krumpen, T.: Improvement and sensitivity analysis of thermal thin-ice retrievals, IEEE Trans. Geosci. Remote Sensing, 51, 3306–3318, 2013.

Aksenov, Y., Ivanov, V. V., Nurser, A. J. G., Bacon, S., Polyakov, I. V., Coward, A. C., Garabato, A. C. N., and Moeller, A. B.: The Arctic circumpolar boundary current, J. Geophys. Res., 116, C09 017, doi:10.1029/2010JC006637, 2011.

Backhaus, J. A., Fohrmann, H., Kaempf, J., and Rubina, A.: Formation and export of water masses produced in Arctic shelf polynyas – Process studies of oceanic convection, J. Mar. Sci., 54, 366–382, 1997.

Baldauf, M.: A new fast-waves solver for the Runge-Kutta dynamical core, Tech. rep., Deutscher Wetterdienst, 2013.

Bareiss, J. and Görgen, K.: Spatial and temporal variability of sea ice in the Laptev Sea: Analyses and review of satellite passive-microwave data and model results, 1979 to 2002, Global Planet. Change, 48, 28–54, doi:10.1016/j.gloplacha.2004.12.004, 2005.

Bauch, D., Schlosser, P., and Fairbanks, R. F.: Freshwater balance and the sources of deep and bottom waters in the Arctic Ocean inferred from the distribution of $H_2^{18}O$, Prog. Oceanogr., 35, 53–80, doi:10.1016/0079-6611(95)00005-2, 1995.

Bauch, D., Dmitrenko, I. A., Wegner, C., Hölemann, J., Kirillov, S. A., Timokhov, L. A., and Kassens, H.: Exchange of Laptev Sea and Arctic Ocean halocline waters in response to atmospheric forcing, J. Geophys. Res., 114, C05 008, doi:10.1029/2008JC005062, 2009.

Bauer, M., Schröder, D., Heinemann, G., Willmes, S., and Ebner, L.: Quantifying polynya ice production in the Laptev Sea with the COSMO model, Polar Res., 32, 20 922, doi:10.3402/polar.v32i0.20922, 2013.

Bowen, I. S.: The ratio of heat losses by conduction and by evaporation for any water surface., Physiol. Rev., 27., 779–787, 1926.

Bromwich, D. H., Hines, K. M., and Bai, L.-S.: Development and testing of Polar Weather Research and Forecasting model: 2. Arctic Ocean, J. Geophys. Res. Atmos., 114, D08 122, doi:10.1029/2008JD010300, 2009.

Dee, D. P., Uppala, S. M., Simmons, A. J., Berrisford, P., Poli, P., Kobayashi, S., Andrae, U., Balmaseda, M. A., Balsamo, G., Bauer, P., Bechtold, P., Beljaars, A. C. M., van de Berg, L., Bidlot, J., Bormann, N., Delsol, C., Dragani, R., Fuentes, M., Geer, A. J., Haimberger, L., Healy, S. B., Hersbach, H., Hólm, E. V., Isaksen, L., Kåberg, P., Köhler, M., Matricardi, M., McNally, A. P., Monge-Sanz, B. M., Morcrette, J.-J., Park, B.-K., Peubey, C., de Rosnay, P., Tavolato, C., Thépaut, J.-N., and Vitart, F.: The ERA-Interim reanalysis: configuration and performance of the data assimilation system, Q. J. Roy. Meteor. Soc., 137, 553–597, doi:10.1002/qj.828, 2011.

Dethleff, D., Loewe, P., and Kleine, E.: The Laptev Sea flaw lead – detailed investigation on ice formation and export during 1991/1992 winter season, Cold. Reg. Sci. Technol., 27, 225–243, doi:10.1016/S0165-232X(98)00005-6, 1998.

Dmitrenko, I., Hölemann, J. A., Tyshko, K., Churun, V., Kirillov, S., and Kassens, H.: The Laptev Sea flaw polynya, Russian Arctic: effects on the mesoscale hydrography, Ann. Glaciol., 33, 373–376, doi:10.3189/172756401781818455, 2001.

Dmitrenko, I. A., Tyshko, K. N., Kirillov, S. A., Eicken, H., Hölemann, J., and Kassens, H.: Impact of flaw polynyas on the hydrography of the Laptev Sea, Global Planet. Change, 48, 9–27, doi:10.1016/j.gloplacha.2004.12.016, 2005.

Dmitrenko, I. A., Kirillov, S. A., Tremblay, L. B., Bauch, D., and Willmes, S.: Sea-ice production over the Laptev Sea shelf inferred from historical summer-to-winter hydrographic observations of 1960s–1990s, Geophys. Res. Lett., 36, L13 605, doi:10.1029/2009GL038775, 2009.

Dmitrenko, I. A., Kirillov, S. A., Bloshkina, E., and Lenn, Y.-D.: Tide-induced vertical mixing in the Laptev Sea coastal polynya, J. Geophys. Res. Oceans, 117, C00G14, doi:10.1029/2011JC006966, 2012.

Doms, G., Förster, J., Heise, E., Herzog, H., Raschendorfer, M., Reinhardt, T., Ritter, B., Schrodin, R., Schulz, J.-P., and Vogel, G.: A Description of the Nonhydrostatic Regional COSMO-Model Part II: Physical Parameterization, Consortium for Small-scale Modelling, Deutscher Wetterdienst, Offenbach, Germany, 2011.

Ebner, L., Schröder, D., and Heinemann, G.: Impact of Laptev Sea flaw polynyas on the atmospheric boundary layer and ice production using idealized mesoscale simulations, Polar Res., 30, 7010, doi:10.3402/polar.v30i0.7210, 2011.

Eicken, H., Dmitrenko, I. A., Tyshko, K., Darovskikh, A., Dierking, W., Blahak, U., Groves, J., and Kassens, H.: Zonation of the Laptev Sea landland ice cover and its importance in a frozen estuary., Glob. Planet. Change, 48, 55–83, doi:10.1016/j.gloplacha.2004.12.005, 2005.

Haid, V., Timmermann, R., Ebner, L., and Heinemann, G.: Atmospheric forcing of coastal polynyas in the south-western Weddell Sea, Antarct. Sci., pp. 1–15, doi:10.1017/S0954102014000893, 2015.

Hall, D., Key, J., Casey, K., Riggs, G., and Cavalieri, D.: Sea ice surface temperature product from MODIS, IEEE Trans. Geosci. Remote Sens., 42, 1076 – 1087, 2004.

Heinemann, G. and Kerschgens, M.: Comparison of methods for area-averaging surface energy fluxes over heterogeneous land surfaces using high-resolution non-hydrostatic simulations, Int. J. Climatol., 25, 379–403, doi:10.1002/joc.1123, 2005.

Heinemann, G. and Rose, L.: Surface energy balance, parameterizations of boundary-layer heights and the application of resistance laws near an Antarctic Ice Shelf front, Boundary Layer Meteorol., 51, 123–158, doi:10.1007/BF00120464, 1990.

Heinemann, G., Helbig, A., and Ernsdorf, T.: Russisch–Deutsche Zusammenarbeit: System Laptev-See, Zwischenbericht 2008, Fahrtbericht der Expedition Transdrift XIII. (Russian–German Cooperation: System Laptev Sea, report 2008, the cruise report of the Transdrift XIII expedition.), chap. Meteorological measurements at the ice edge of the West New Siberian Polynya, pp. 8–19, IFM-GEOMAR, 2009.

Hines, K. M., Bromwich, D. H., Bai, L., Bitz, C. M., Powers, J. G., and Manning, K. W.: Sea Ice Enhancements to Polar WRF, Mon. Weather Rev., doi:10.1175/MWR-D-14-00344.1, 2015.

Ivanov, V. V. and Golovin, P.: Observations and modeling of dense water cascading from the northwestern Laptev Sea, J. Geophys. Res., 112, C09 003, doi:10.1029/2006JC003882, 2007.

Iwamoto, K., Ohshima, K. I., and Tamura, T.: Improved mapping of sea ice production in the Arctic Ocean using AMSR-E thin ice thickness algorithm, J. Geophys. Res. Oceans, 119, 3574–3594, doi:10.1002/2013JC009749, http://onlinelibrary.wiley.com/doi/10.1002/2013JC009749/abstract, 2014.

Johnson, M. A. and Polyakov, I. V.: The Laptev Sea as a source for recent Arctic Ocean salinity changes, Geophys. Res. Lett., 28, 2017–2020, doi:10.1029/2000GL012740, 2001.

Køltzow, M.: The effect of a new snow and sea ice albedo scheme on regional climate model simulations, J. Geophys. Res., 112, D07 110, doi:10.1029/2006JD007693, 2007.

Krumpen, T., Hölemann, J. A., Willmes, S., Morales Maqueda, M. A., Busche, T., Dmitrenko, I. A., Gerdes, R., Haas, C., Heinemann, G., Hendricks, S., Kassens, H., Rabenstein, L., and Schröder, D.: Sea ice production and water mass modification in the eastern Laptev Sea, J. Geophys. Res., 116, C05 014, doi:10.1029/2010JC006545, 2011.

Krumpen, T., Janout, M., Hodges, K. I., Gerdes, R., Girard-Ardhuin, F., Hölemann, J. A., and Willmes, S.: Variability and trends in Laptev Sea ice outflow between 1992–2011, Cryosphere, 7, 349–363, doi:10.5194/tc-7-349-2013, 2013.

Launiainen, J. and Vihma, T.: Derivation of turbulent surface fluxes - An iterative flux-profile method allowing arbitrary observing heights, Environ. Softw., 5, 113–124, doi:10.1016/02669838(90)90021-w, 1990.

Louis, J.-F.: A parametric model of vertical eddy fluxes in the atmosphere, Boundary Layer Meteorol., 17, 187–202, doi:10.1007/BF00117978, 1979.

Lüpkes, C. and Gryanik, V. M.: A stability dependent parametrization of transfer coefficients for momentum and heat over polar sea ice to be used in climate models, J. Geophys. Res. Atmos., p. 2014JD022418, doi:10.1002/2014JD022418, 2014.

5 Markus, T. and Burns, B. A.: A method to estimate subpixel-scale coastal polynyas with satellite passive microwave data, J. Geophys. Res. Oceans, 100, 4473–4487, doi:10.1029/94JC02278, 1995.

Martin, S. and Cavalieri, D.: Contributions of the Siberian shelf polynyas to the Arctic Ocean intermediate and deep water, J. Geophys. Res. Oceans, 94, 12 725–12 738, doi:10.1029/JC094iC09p12725, 1989.

Martin, S. and Kauffmann, P.: A field and laboratory study of wave dumping by grease ice, J. Glacial., 27, 293–313, 1981.

10 Massom, R. A., Harris, P. T., Michael, K. J., and Potter, M.: The distribution and formative processes of latent-heat polynyas in East Antarctica, Ann. Glaciol., 27, 420–426, 1998.

Mellor, G. L. and Yamada, T.: A Hierarchy of Turbulence Closure Models for Planetary Boundary Layers, J. Atmos. Sci., 31, 1791–1806, doi:10.1175/1520-0469(1974)031<1791:AHOTCM>2.0.CO;2, 1974.

Mironov, D., Ritter, B., Schulz, J.-P., Buchhold, M., Lange, M., and Machulskaya, E.: Parameterisation of sea and lake ice in numerical
15   weather prediction models of the German Weather Service, Tellus A, 64, 17 330, doi:10.3402/tellusa.v64i0.17330, 2012.

Morales Maqueda, M. A., Willmott, A. J., and Biggs, N. R. T.: Polynya Dynamics: a Review of Observations and Modeling, Rev. Geophys., 42, RG1004, doi:10.1029/2002RG000116, 2004.

Paul, S., Willmes, S., Gutjahr, O., Preußer, A., and Heinemann, G.: Spatial Feature Reconstruction of Cloud-Covered Areas in Daily MODIS Composites, Rem. Sens., 7, 5042–5056, doi:10.3390/rs70505042, http://www.mdpi.com/2072-4292/7/5/5042, 2015.

20 Perovich, D. K. and Grenfell, T. C.: Laboratory studies of the optical properties of young sea ice, J. Glacial., 27, 331–346, 1981.

Persson, P. O. G., Fairall, C. W., Andreas, E. L., Guest, P., and D., K.: Measurements near the Atmospheric Surface Flux Group tower at SHEBA: Near-surface conditions and surface energy budget, J. Geophys. Res., 107(C10), 8045, doi:10.1029/2000JC000705, 2002.

Preußer, A., Heinemann, G., and Willmes: Multi-Decadal variability of Thin-Ice Dynamics and Ice Production in the North Water Polynya by means of Passive Microwave and Thermal Infrared Satellite Imagery, Rem. Sens., 7(12), 15 844–15 867, doi:10.3390/rs71215807, 2015a.

25 Preußer, A., Willmes, S., Heinemann, G., and Paul, S.: Thin-ice dynamics and ice production in the Storfjorden polynya for winter-seasons 2002/2003–2013/2014 using MODIS thermal infrared imagery, Cryosphere, 9, 1063–1073, doi:10.5194/tcd-8-5763-2014, 2015b.

Riggs, G., Hall, D., and Salomonson, V.: MODIS Sea Ice Products User Guide to Collection 5, NSIDC, 2006.

Rigor, I. G. and Colony, R. L.: Sea-ice production and transport of pollutants in the Laptev Sea, Sci. Total Environ., 202, 89–110, 1997.

Ritter, B. and Geleyn, J.-F.: A Comprehensive Radiation Scheme for Numerical Weather Prediction Models with Potential Applications in
30   Climate Simulations, Mon. Weather Rev., 120, 303–325, doi:10.1175/1520-0493(1992)120<0303:ACRSFN>2.0.CO;2, 1992.

Rockel, B., Will, A., and Hense, A.: The Regional Climate Model COSMO-CLM (CCLM), Met. Z., 17(4), 347–348, 2008.

Rudels, B., Friedrich, H. J., and Quadfasel, D.: The Arctic circumpolar boundary current, Deep Sea Res., 46, 1023–1062, doi:10.1016/S0967-0645(99)00015-6, 1999.

Schröder, D., Vihma, T., Kerber, A., and Brümmer, B.: On the parameterization of turbulent surface fluxes over heterogeneous sea ice
35   surfaces, J. Geophys. Res. Oceans, 108, 3195, doi:10.1029/2002JC001385, 2003.

Schröder, D., Heinemann, G., and Willmes, S.: The impact of a thermodynamic sea-ice module in the COSMO numerical weather prediction model on simulations for the Laptev Sea, Siberian Arctic, Polar Res., 30, 6334, doi:10.3402/polar.v30i0.6334, 2011.

Schweiger, A., Lindsay, R., Zhang, J., Steele, M., Stern, H., and Kwok, R.: Uncertainty in modeled Arctic sea ice volume, J. Geophys. Res. Oceans, 116, C00D06, doi:10.1029/2011JC007084, 2011.

Smedsrud, L. H. and Martin, T.: Grease ice in basin-scale sea-ice ocean models, Ann. Glaciol., 56(69), 295–306, doi:10.3189/2015AoG69A765, 2015.

5 Smith, S. D., Muench, R. D., and Pease, C. H.: Polynyas and leads: An overview of physical processes and environment, J. Geophys. Res. Oceans, 95, 9461–9479, doi:10.1029/JC095iC06p09461, 1990.

Spreen, G., Kaleschke, L., and Heygster, G.: Sea ice remote sensing using AMSR-E 89-GHz channels, J. Geophys. Res. Oceans, 113, C02S03, doi:10.1029/2005JC003384, 2008.

Steppeler, J., Doms, G., Schättler, U., Bitzer, H. W., Gassmann, A., Damrath, U., and Gregoric, G.: Meso-gamma scale forecasts using the
10 nonhydrostatic model LM, Meteor. Atmos. Phys., 82, 75–96, doi:10.1007/s00703-001-0592-9, 2003.

Tamura, T. and Ohshima, K. I.: Mapping of sea ice production in the Arctic coastal polynyas, J. Geophys. Res. Oceans, 116, C07 030, doi:10.1029/2010JC006586, http://onlinelibrary.wiley.com/doi/10.1029/2010JC006586/abstract, 2011.

Timokhov, L. A.: Regional characteristics of the Laptev and the East Siberian seas: climate, topography, ice phases, thermohaline regime, circulation., Ber. Polarforsch., 114, 15–32, http://epic.awi.de/26322/1/BerPolarforsch1994144.pdf, 1994.

15 Uttal, T., Curry, J. A., Mcphee, M. G., Perovich, D. K., Moritz, R. E., Maslanik, J. A., Guest, P. S., Stern, H. L., Moore, J. A., Turenne, R., Heiberg, A., Serreze, M. C., Wylie, D. P., Persson, O. G., Paulson, C. A., Halle, C., Morison, J. H., Wheeler, P. A., Makshtas, A., Welch, H., Shupe, M. D., Intrieri, J. M., Stamnes, K., Lindsey, R. W., Pinkel, R., Pegau, W. S., Stanton, T. P., and Grenfeld, T. C.: Surface Heat Budget of the Arctic Ocean, Bull. Am. Meteorol. Soc., 83, 255–275, doi:10.1175/1520-0477(2002)083<0255:SHBOTA>2.3.CO;2, 2002.

Van Pham, T., Brauch, J., Dieterich, C., Frueh, B., and Ahrens, B.: New coupled atmosphere-ocean-ice system COSMO-CLM/NEMO:
20 assessing air temperature sensitivity over the North and Baltic Seas, Oceanologia, 56, 167–189, doi:10.5697/oc.56-2.167, 2014.

Vihma, T.: Subgrid parameterization of surface heat and momentum fluxes over polar oceans, J. Geophys. Res. Oceans, 100, 22 625–22 646, doi:10.1029/95JC02498, 1995.

Wicker, L. J. and Skamarock, W. C.: Time-Splitting Methods for Elastic Models Using Forward Time Schemes, Mon. Weather Rev., 130, 2088–2097, doi:10.1175/1520-0493(2002)130<2088:TSMFEM>2.0.CO;2, http://journals.ametsoc.org/doi/abs/10.
25 1175/1520-0493(2002)130%3C2088%3ATSMFEM%3E2.0.CO%3B2, 2002.

Willmes, S., Krumpen, T., Adams, S., Rabenstein, L., and Haas, C.: Cross-validation of polynya monitoring methods from multi-sensor satellite and airborne data: A case study., Can. J. Remote Sens., pp. 196–210, doi:10.5589/m10-012, 2010.

Willmes, S., Adams, S., Schröder, D., and Heinemann, G.: Spatio-temporal variability of polynya dynamics and ice production in the Laptev Sea between the winters of 1979/80 and 2007/08, Polar Res., 30, 5971, doi:10.3402/polar.v30i0.5971, 2011.

30 Yu, Y. and Lindsay, R.: Comparison of thin ice thickness distributions derived from RADARSAT Geophysical Processor System and advanced very high resolution radiometer data sets, J. Geophys. Res., 108, 3387, 2003.

Yu, Y. and Rothrock, D. A.: Thin ice thickness from satellite thermal imagery, J. Geophys. Res., 101, 25 753–25 766, 1996.

Zhang, J. and Rothrock, D. A.: Modeling Global Sea Ice with a Thickness and Enthalpy Distribution Model in Generalized Curvilinear Coordinates, Mon. Weather Rev., 131, 845–861, doi:10.1175/1520-0493(2003)131<0845:MGSIWA>2.0.CO;2, 2003.